Magnetic impurity as a local probe of the $U(1)$ quantum spin liquid with spinon Fermi surface

Wen-Yu He [1,2,*] and Patrick A. Lee[2,†]

[1]*School of Physical Science and Technology, ShanghaiTech University, Shanghai 201210, China*
[2]*Department of Physics, Massachusetts Institute of Technology, Cambridge, Massachusetts 02139, USA*

We solve the problem of a magnetic impurity coupled to a $U(1)$ quantum spin liquid with a spinon Fermi surface, and we compute the impurity spectral function. Using the slave rotor mean-field approach combined with gauge field fluctuations, we find that a peak located at the top of the lower Hubbard band and one at the bottom of the upper Hubbard band can emerge in the impurity spectral function. The peaks at the Hubbard band edges arise from the gauge field fluctuation-induced spinon-chargon binding inside the spinon Kondo screening cloud of the magnetic impurity. For a magnetic impurity embedded in a Mott insulator, our findings suggest that the emergence of a pair of peaks at the Hubbard band edges in the impurity density of states spectra provides strong evidence that the host Mott insulator is a $U(1)$ quantum spin liquid with a spinon Fermi surface.

I. INTRODUCTION

The Anderson impurity model describes how a local atomic impurity interacts with electrons in its host system [1]. The most well studied case is a magnetic impurity embedded in a nonmagnetic metal, where the Coulomb repulsion at the impurity suppresses the charge fluctuations, but the local magnetic moment can freely couple with spins of nearby conducting electrons in the metal [2]. The Anderson model of a magnetic impurity can be reduced to the Kondo model [2,3] that focuses on the spin interaction between the impurity and the nearby electrons. Below the Kondo temperature T_K, the conducting electron spins form the Kondo cloud to screen the local magnetic moment [4–8], and a correlated electronic state develops at the impurity. The correlated state is characterized by a narrow peak, known as the Kondo resonance [2,5], which always shows up at the Fermi energy in the impurity electronic spectral function. Therefore, the Kondo resonance has become the fingerprint for the correlation phenomenon induced by a magnetic impurity on a metallic host [9,10].

The thorough study of a magnetic impurity on a metallic host has stimulated further interest to generalize the non-interacting metallic host to a quantum system with strong electron-electron interaction, such as quantum spin liquid (QSL) [11–18]. As the magnetic impurity couples with the electronic states locally in the QSL host, the correlated many-body ground state in the QSL is expected to affect the quantum state at the impurity. In this way, the magnetic impurity acts as a local probe of the QSL. Among QSLs with various gauge groups [19–21], the $U(1)$ QSL with a spinon Fermi surface (SFS) is particularly interesting, and recently TaS_2 and monolayer $TaSe_2$ have been studied as candidates for the $U(1)$ QSL with SFS [22–31]. Furthermore, it has

been shown to be experimentally possible to deposit magnetic impurities on the monolayer $TaSe_2$ surface and perform local spectroscopy measurements on the magnetic impurity [32]. Since scanning tunneling spectroscopy (STS) has been proven to be a direct experimental way [33] to study the physics of a magnetic impurity on an electronic Fermi liquid metal, the analogous problem of the STS spectrum when a magnetic impurity is coupled to a $U(1)$ QSL with SFS becomes a key problem that needs to be theoretically solved. While the possibility of Kondo screening by a spinon Fermi surface has previously been addressed [14], the tunneling density of states has not been calculated. This is the main goal of this paper.

The $U(1)$ QSL with SFS is a Mott insulator with no magnetic order down to zero temperature [19–21]. In the $U(1)$ QSL with SFS, the electrons go through spin-charge separation and are decomposed into spinons and chargons, with an emergent $U(1)$ gauge field to couple both [34]. The spinons are charge-neutral spin-1/2 excitations living on a Fermi surface, while the chargons are gapped spinless bosons that carry electric charges. For a magnetic impurity embedded on a $U(1)$ QSL with SFS, since the spinons in the QSL are itinerant, the magnetic impurity can have spin exchange freely with the itinerant spinons nearby, and the Kondo model that involves the spin degree coupling has been applied to study the system [14].

In the Kondo model description for the magnetic impurity on a $U(1)$ QSL with SFS, the itinerant spinons in the QSL take the role of the spin-1/2 conducting electrons in the metal, so it was predicted and further supported by experimental evidence that a spinon cloud can form around the magnetic impurity to screen the local magnetic moment [14,15], similar to the conventional Kondo phenomenon in a metallic host. However, unlike the conventional Kondo problem where the impurity magnetic moment couples to the spin of charged electrons in the metallic host, the Kondo model adopted in the $U(1)$ QSL host only takes into account the spinons that carry no charge. Since the local spectroscopy measurements on the magnetic

*hewy@shanghaitech.edu.cn
†palee@mit.edu

impurity involve the physical electron transfer that contains both the spin and charge degree, the Kondo model used in the QSL host [14] becomes insufficient to generate the impurity electronic spectral function.

In this work, we obtain the impurity electronic spectral function of a magnetic impurity embedded in a $U(1)$ QSL with SFS by solving the Anderson impurity model, which considers both the spin and charge degree of electrons. The slave rotor mean-field theory [35,36] is applied to deal with the Anderson impurity model. At the magnetic impurity, the electron is decomposed into a spin-1/2 auxiliary fermion (SAF) and a charged boson (CB), which couples with the spinons and chargons in the QSL, respectively. The coupling of the SAF and the spinons corresponds to the Kondo model that contains only the spin degree, generating the resonance at the spinon Fermi energy in the SAF spectral function. The coupling of the CB and the chargons fills in the missing charge degree of the Kondo model. At the mean-field level with no gauge field fluctuations in the QSL, the impurity electronic spectral function obtained from the slave rotor treatment involves the QSL chargon density of states (DOS) in addition to the original atomic energy levels, so the magnetic impurity on a $U(1)$ QSL with SFS locally provides information on the QSL chargon DOS.

In a $U(1)$ QSL, the spinons and chargons both couple to an emergent $U(1)$ gauge field, so the quantum fluctuations of the $U(1)$ gauge field affect the low-energy excitations in the QSL. In a two-dimensional $U(1)$ QSL with a gapped spinon spectrum, it is known from Polyakov that the low-energy effective theory of the QSL is a pure compact $U(1)$ gauge theory that is always confining. As a result, an arbitrary coupling to the $U(1)$ gauge field gives rise to confinement of spinons [37]. However, in a $U(1)$ QSL with a gapless spinon spectrum, since the gapless matter field damps the gauge field, the situation becomes different. In a $U(1)$ QSL with a Dirac spinon band dispersion, it has been found that when the physical $SU(2)$ spin is generalized to $SU(N)$, deconfinement of spinons is possible for a sufficiently large N [38]. In our case of a two-dimensional $U(1)$ QSL with SFS, due to the many gapless spinon excitations from the SFS, a noncompact $U(1)$ gauge theory applies to describe the low-energy excitations, and it becomes possible to have deconfinement of spinons [39]. In the rest of the paper, deconfinement of spinons is a prerequisite for the treatment of gauge field fluctuations that we apply to the two-dimensional $U(1)$ QSL with SFS.

In a two-dimensional $U(1)$ QSL with SFS, as the spinons and chargons both couple to an emergent $U(1)$ gauge field, the gauge field fluctuations can generate a binding interaction between a spinon and a chargon [40,41]. In the spinon Kondo cloud around the magnetic impurity, the spinon-chargon binding interaction is found to induce the spectral weight to transfer from the bulk Hubbard bands to the Hubbard band edges, so a band-edge resonance peak arises at the top of the lower Hubbard band (LHB) and one arises at the bottom of the upper Hubbard band (UHB) in the impurity spectral function. When the spinon-chargon binding interaction is sufficiently large, the pair of band-edge resonance peaks can further move inside the Mott gap and become in-gap bound state peaks. Due to the spinon Kondo cloud of the magnetic impurity and the spinon-chargon binding interaction inside, the magnetic

impurity embedded on a $U(1)$ QSL with SFS behaves like an impurity of acceptor and donor type simultaneously and induces a pair of peaks at the Hubbard band-edge energies. As a result, in the spectroscopy of the magnetic impurity, the emergence of a peak at both the UHB bottom and LHB top provides strong evidence that the host Mott insulator is a $U(1)$ QSL with SFS.

The rest of the paper is organized as follows: In Sec. II, the slave rotor mean-field theory to solve the Anderson impurity model is introduced. In Sec. III, a magnetic impurity weakly coupled to a $U(1)$ QSL with SFS is analyzed in both the SAF spinon coupling channel and the CB chargon coupling channel. The impurity bare electronic spectral function, which does not consider the gauge field fluctuations, is analytically derived. The resulting impurity bare electronic spectral function is shown to measure the chargon DOS in the QSL host. In Sec. VI, a full numerical self-consistent mean-field calculation for a magnetic impurity embedded in a $U(1)$ QSL with SFS of a triangular lattice is carried out. The impurity bare electronic spectral function obtained numerically confirms that a magnetic impurity on a $U(1)$ QSL with SFS probes the chargon DOS in the QSL, under the condition that the QSL has negligible gauge field fluctuations. In Sec. V, the gauge field fluctuations in the QSL are taken into account and the effect is to bring about the spinon-chargon binding interaction in the QSL. Around the magnetic impurity, the binding of a spinon state in the spinon Kondo cloud and a chargon makes the magnetic impurity become an impurity of acceptor and donor type simultaneously, giving rise to a peak located at the UHB bottom and one at the LHB top in the impurity spectral function. The pair of peaks are either band-edge resonance peaks inside the Hubbard bands or in-gap peaks of the formed bound states, depending on the binding interaction strength. In Sec. VI, our findings about the magnetic impurity on a $U(1)$ QSL with SFS are summarized, and the connection to experimental spectroscopy measurements of a magnetic impurity on a Mott insulator is constructed.

II. THE SLAVE ROTOR MEAN-FIELD THEORY FOR THE IMPURITY MODEL

The Hamiltonian for a local atomic impurity with on-site Coulomb repulsion U takes the form

$$H_{\mathrm{d}} = \sum_{\sigma} \epsilon_0 d_{\sigma}^{\dagger} d_{\sigma} + \frac{U}{2} \left(\sum_{\sigma} d_{\sigma}^{\dagger} d_{\sigma} - 1 \right)^2.$$

Here ϵ_0 is the impurity on-site energy, and $\sigma = \uparrow / \downarrow$ is the spin index. In the slave rotor formalism [35,36], the electronic operator at the impurity is rewritten as $d_{\sigma}^{\dagger} = a_{\sigma}^{\dagger} e^{i\theta}$, $d_{\sigma} = a_{\sigma} e^{-i\theta}$, where $a_{\sigma}^{(\dagger)}$ is the annihilation (creation) operator for a SAF, and $e^{\pm i\theta}$ is the rotor to represent the charge degree of the impurity electron. In the slave rotor representation, the angular momentum $L = -i \frac{\partial}{\partial \theta}$ is introduced to express the Coulomb repulsion term in H_d as $\frac{U}{2} L^2$, under the constraint $L = \sum_{\sigma} a_{\sigma}^{\dagger} a_{\sigma} - 1$. As the angular momentum L and the rotor phase variable θ respect the canonical commutation $[\theta, L] = i$, the action for the impurity can be constructed from $S = \int_0^{\beta} (-iL \partial_{\tau} \theta + \sum_{\sigma} a_{\sigma}^{\dagger} a_{\sigma} + H_d) d\tau$. After an integration
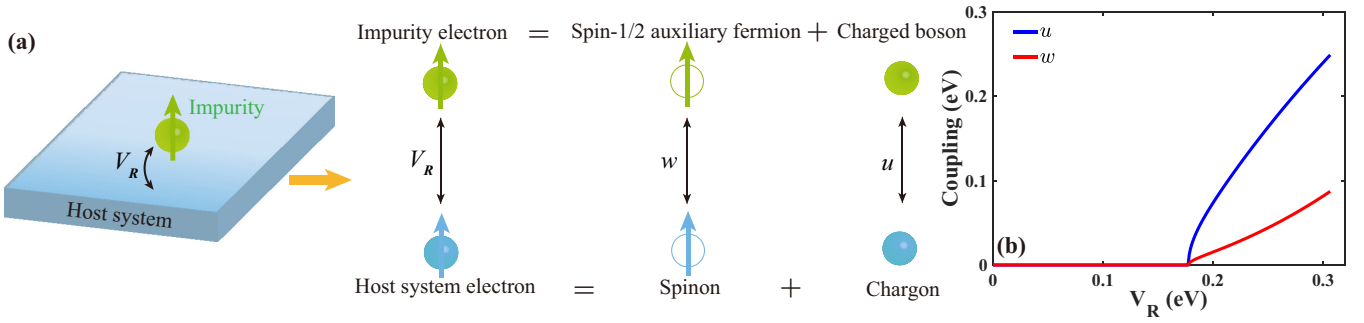
FIG. 1. (a) A magnetic impurity embedded in a host system and the slave rotor mean-field description for the system. In the slave rotor representation, the electronic state at the magnetic impurity is decomposed into a SAF and a CB, while the electrons in the host system are decomposed into spinons and chargons. The SAF has the mean-field coupling w with the spinons, and the CB takes the mean-field coupling u with the chargons. The mean-field couplings w and u are developed from the original electronic coupling V_R. (b) The mean-field coupling parameters w and u as a function of the electronic coupling V_R for a magnetic impurity on a $U(1)$ QSL with SFS. The QSL is of triangular lattice. As V_R increases, both w and u take significant nonzero values.

over L, we get the action for the local atomic impurity as [35]

$$S_d = \int_0^\beta \left[\frac{1}{U}(\partial_\tau + h)X_d^\dagger(\partial_\tau - h)X_d \right.$$

$$\left. + \sum_\sigma a_\sigma^\dagger(\partial_\tau + \epsilon_0 - h)a_\sigma + \lambda(X_d^\dagger X_d - 1) + h \right]d\tau, \quad (1)$$

with $X_d^\dagger = e^{-i\theta}$, $X_d = e^{i\theta}$ interpreted as the charged bosonic operator at the impurity, λ is the Lagrangian multiplier to guarantee $X_d^\dagger X_d = 1$, and h is the Lagrangian multiplier to implement the constraint $L = \sum_\sigma a_\sigma^\dagger a_\sigma - 1$. In the action S_d, the impurity electron has been decomposed into a SAF and a CB, which can couple with external spin and charge degrees individually.

Embedded on a host system, the atomic impurity couples with the host, yielding the coupling action

$$S_c = \int_0^\beta \sum_\sigma V_R(f_{\sigma,R}^\dagger a_\sigma X_d^\dagger X_R + a_\sigma^\dagger f_{\sigma,R} X_R^\dagger X_d)d\tau, \quad (2)$$

where V_R is the electronic coupling with the nearest-neighbor site R in the host system. Here the electrons in the host system have been expressed in the slave rotor representation as well: $c_{\sigma,r}^\dagger = f_{\sigma,r}^\dagger X_r$, $c_{\sigma,r} = f_{\sigma,r} X_r^\dagger$, with $f_{\sigma,r}^{(\dagger)}$, $X_r^{(\dagger)}$ to

annihilate (create) a spinon and chargon, respectively, at the site r. The spinon is a chargeless spin-$1/2$ fermion, and the chargon is a spinless CB, representing the spin degree and the charge degree of an electron in the host, respectively. With the imaginary-time Green's function $G_{f,\sigma}(\tau, \tau', r, r')$ and $G_X(\tau, \tau', r, r')$ for the spinon and chargon, respectively, the action for the host system can be written as

$$S_h = -\int_{\tau,\tau',r,r'} \sum_\sigma f_{\sigma,r}^\dagger(\tau) G_{f,\sigma}^{-1}(\tau, \tau', r, r') f_{r',\sigma}(\tau')$$

$$+ \int_{\tau,\tau',r,r'} X_r^\dagger(\tau) G_X^{-1}(\tau, \tau', r, r') X_{r'}(\tau'), \quad (3)$$

with $\int_{\tau,\tau',r,r'} \equiv \int_0^\beta d\tau \int_0^\beta d\tau' \int dr \int dr'$.

Now it is ready to have the total action for an atomic impurity embedded on a host system as $S_{tot} = S_d + S_c + S_h$. In the total action S_{tot}, all terms are quadratic except the ones in S_c, so the mean-field parameters w for the SAF spinon coupling, and u for the CB chargon coupling, are introduced through the Hubbard-Stratonovich transformation to decouple the quartic terms in S_c. Eventually, the action for the whole system takes the form

$$S_0 = \int_0^\beta \left[\sum_\sigma a_\sigma^\dagger(\partial_\tau + \epsilon_0 - h)a_\sigma + \frac{\partial_\tau X_d^\dagger \partial_\tau X_d}{U} + \frac{h}{U}(X_d^\dagger \partial_\tau X_d - X_d \partial_\tau X_d^\dagger) + \lambda(X_d^\dagger X_d - 1) + h - \frac{h^2}{U} \right]d\tau$$

$$- \int_0^\beta d\tau \int_0^\beta d\tau' \int dr \int dr' \sum_\sigma [f_{\sigma,r}^\dagger(\tau) G_{f,\sigma}^{-1}(\tau, \tau', r, r') f_{r',\sigma} - X_r^\dagger(\tau) G_X^{-1}(\tau, \tau', r, r') X_{r'}(\tau)]$$

$$+ \int_0^\beta \left[\frac{2uw}{V_R} + w(f_{\sigma,R}^\dagger a_\sigma + a_\sigma^\dagger f_{\sigma,R}) - u(X_d^\dagger X_R + X_R^\dagger X_d) \right]d\tau. \quad (4)$$

In this slave rotor treatment, the coupling of the impurity electron and the electronic states in the host has been decomposed into two individual channels: the SAF has the coupling w with the spinons, and the CB takes the coupling u with the chargons. The mean-field coupling parameters w and u

are controlled by the electronic coupling V_R. For an atomic impurity embedded in a host system, the decomposition of electronic coupling into the SAF spinon coupling channel and the CB chargon coupling channel is schematically shown in Fig. 1(a). With a given spinon and chargon Green's function

in the host system, the action in Eq. (4) is generally applicable to a local atomic impurity embedded on a host, regardless of whether the host system is a metal or a QSL.

In the mean-field theory, the coupling fields w, u and the Lagrangian multipliers λ, h take the value at the saddle point where the free energy for the whole system gets minimized. After the Fourier transformation to the Matsubara frequency space, the self-consistent equations that determine the value of w, u, λ, and h are

$$u = -\frac{2wV_{\boldsymbol{R}}}{\beta} \sum_{\omega_n} G_{a,\sigma}(i\omega_n) G_{f,\sigma}(i\omega_n, \boldsymbol{R}, \boldsymbol{R}), \quad (5)$$

$$w = \frac{uV_{\boldsymbol{R}}}{\beta} \sum_{v_n} G_{X_d}(iv_n) G_X(iv_n, \boldsymbol{R}, \boldsymbol{R}), \quad (6)$$

$$1 = \frac{1}{\beta} \sum_{v_n} G_{X_d}(iv_n) e^{iv_n 0^+}, \quad (7)$$

$$\frac{1}{2} - \frac{h}{U} = \frac{1}{2U\beta} \sum_{v_n} iv_n G_{X_d}(iv_n)[e^{iv_n 0^+} + e^{-iv_n 0^+}]$$
$$+ \frac{1}{\beta} \sum_{\omega_n} G_{a,\sigma}(i\omega_n) e^{i\omega_n 0^+}, \quad (8)$$

with the SAF Matsubara Green's function

$$G_{a,\sigma}(i\omega_n) = \frac{1}{i\omega_n - \epsilon_0 + h - w^2 G_{f,\sigma}(i\omega_n, \boldsymbol{R}, \boldsymbol{R})}, \quad (9)$$

and the CB Matsubara Green's function

$$G_{X_d}(iv_n) = \frac{1}{\frac{v_n^2}{U} - \frac{2iv_n h}{U} + \lambda - u^2 G_X(iv_n, \boldsymbol{R}, \boldsymbol{R})}. \quad (10)$$

Here $G_{f,\sigma}(i\omega_n, \boldsymbol{R}, \boldsymbol{R})$ and $G_X(iv_n, \boldsymbol{R}, \boldsymbol{R})$ are the Matsubara Green's functions for the spinon and chargon at $\boldsymbol{R}$, respectively, $\omega_n = \frac{(2n+1)\pi}{\beta}$ and $v_n = \frac{2n\pi}{\beta}$ denote the fermionic and bosonic Matsubara frequencies, respectively, and $k_{\rm b}$ in $\beta^{-1} = k_{\rm b}T$ is the Boltzmann constant. Equations (5) and (6) show how the mean-field couplings w and u arise from the electronic coupling $V_{\boldsymbol{R}}$, while Eqs. (7) and (8) determine the chemical potential for the SAF and the CB at the impurity.

Importantly, for an atomic impurity with given on-site energy ϵ_0, Coulomb repulsion U, electronic coupling $V_{\boldsymbol{R}}$, and the Green's functions $G_{f,\sigma}(i\omega_n, \boldsymbol{R}, \boldsymbol{R})$, $G_X(iv_n, \boldsymbol{R}, \boldsymbol{R})$ for the host system, all the mean-field parameters w, u, λ, and h can be self-consistently solved from Eqs. (5)–(8). For the magnetic impurity embedded in a $U(1)$ QSL with SFS with which we are concerned, the mean-field equations will be numerically solved to yield the SAF spinon coupling w and the CB chargon coupling u as a function of the electronic coupling $V_{\boldsymbol{R}}$, which is shown in Fig. 1(b). At the mean-field level where all gauge field fluctuations are neglected, the impurity bare electronic Matsubara Green's function $G^0_{d,\sigma}(i\omega_n)$ is constructed from the convolution

$$G^0_{d,\sigma}(i\omega_n) = \frac{1}{\beta} \sum_{v_n} G_{a,\sigma}(i\omega_n + iv_n) G_{X_d}(iv_n), \quad (11)$$

and the impurity bare electronic spectral function takes the form $\rho^0_d(\omega) = -\frac{1}{\pi} \text{Im} G^0_{d,\sigma}(i\omega_n \to \omega + i0^+)$. We refer to the Green's function and the spectral function as bare because

the spinon-chargon binding has not yet been taken into account. Therefore, the bare spectral function $\rho^0_{d,\sigma}(\omega)$ gives the bare electronic DOS of a magnetic impurity based on a $U(1)$ QSL with SFS, which is the result in the absence of gauge field fluctuations.

III. THE MAGNETIC IMPURITY WEAKLY COUPLED TO THE QSL

The full analytical solution to Eqs. (5)–(8) in the presence of nonzero electronic coupling $V_{\boldsymbol{R}}$ is difficult to obtain, but at weak coupling $V_{\boldsymbol{R}}$ we can make approximations to first get the impurity bare electronic spectral function. Since the weak coupling to the host system has a negligible effect on the occupation of the atomic impurity, the Lagrangian multipliers h and λ, which determine the chemical potential for the SAF and the CB at the impurity, can be approximated by the value in the isolated magnetic impurity case.

By taking $u = 0$ and $w = 0$ in Eqs. (7) and (8), we obtain $h = \epsilon_0$ and $\lambda = \frac{U}{4} - \frac{h^2}{U}$ under the condition $|\epsilon_0| < \frac{1}{2}U$ [35], which corresponds to an isolated single occupied atomic impurity that carries a local magnetic moment. The Matsubara Green's function for the SAF and the CB can accordingly be obtained from Eqs. (9) and (10), respectively. In such an isolated magnetic impurity, the SAF has its energy level right at the Fermi energy, indicating that the local spin at the impurity can have free exchange with external spins, as is schematically shown in Fig. 2(a). On the other hand, the CB at the impurity has two energy levels gapped by the Coulomb repulsion U, denoted by the solid green lines in Fig. 2(b). The CB and the SAF together compose the impurity electron, and the electronic spectrum has the atomic energy levels at $\omega = \epsilon_0 \pm \frac{U}{2}$, as is shown schematically by the solid spectrum in Fig. 2(c). The gapped electronic spectrum at the magnetic impurity indicates that extra charging energy is needed to remove or add an electron into the impurity, so the charge fluctuations are suppressed by the gap. However, since the isolated magnetic impurity has the same energy for the spin-up and spin-down electronic states, the impurity spin can fluctuate freely.

With the approximated Lagrangian multipliers $h = \epsilon_0$ and $\lambda = \frac{U}{4} - \frac{h^2}{U}$ taken from the isolated magnetic impurity model, the coupling u in the CB chargon channel and the coupling w in the spin-1/2 auxiliary fermion spinon channel can be determined by Eqs. (5) and (6), respectively. For a $U(1)$ QSL with SFS as the base for the magnetic impurity, the spinon Green's function takes the form $G_{f,\sigma}(i\omega_n, \boldsymbol{R}, \boldsymbol{R}) = \sum_{\boldsymbol{k}} \frac{1}{i\omega_n - \xi_{\boldsymbol{k}}}$ with the spinon band dispersion $\xi_{\boldsymbol{k}} \in [-\Lambda_f, \Lambda_f]$, and the chargon Green's function is $G_X(iv_n, \boldsymbol{R}, \boldsymbol{R}) = \sum_{\boldsymbol{k}} (\frac{1}{iv_n + \epsilon_{\boldsymbol{k}}} - \frac{1}{iv_n - \epsilon_{\boldsymbol{k}}})$, given the chargon band dispersion $\epsilon_{\boldsymbol{k}} \in [\Delta, \Lambda_X]$ (see Appendix A for more details about the Green's function). By assuming the constant DOS for both the spinon and chargon bands for simplicity, Eqs. (5) and (6), which contain an infinite summation series, are further approximated by two algebra equations,

$$u \approx -\frac{wV_{\boldsymbol{R}}}{2\Lambda_f} \ln \frac{\Gamma_{\rm eff}^2}{\Lambda_f^2 + \Gamma_{\rm eff}^2}, \quad w \approx \frac{4uV_{\boldsymbol{R}}U}{U^2 - 4\epsilon_0^2}, \quad (12)$$
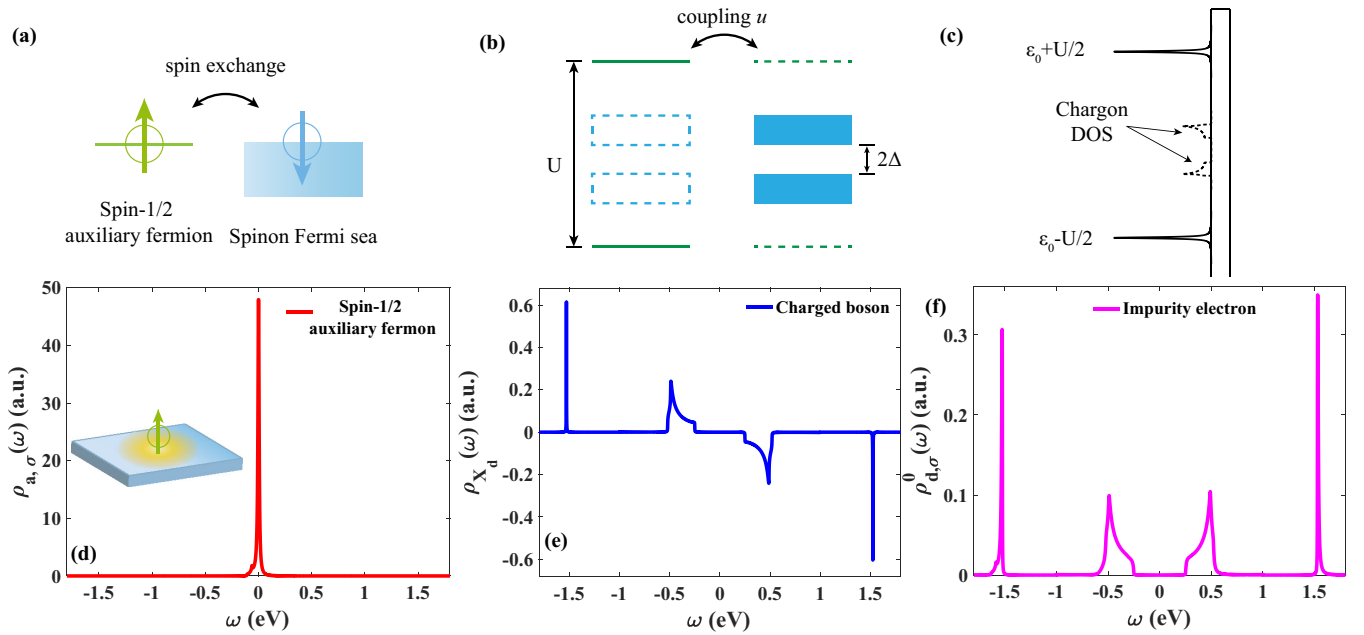
FIG. 2. (a) The spin exchange between the SAF at the impurity and the itinerant spinons in the $U(1)$ QSL with SFS. The impurity SAF lies at the Fermi level and can freely exchange spin with the QSL spinons in the Fermi sea. (b) The energy diagram of the CB at the impurity and the chargons in the QSL. In the absence of the mean-field coupling u, the CB has two energy levels denoted by the solid green lines, which are separated by the Coulomb repulsion U. The chargon energy bands are denoted by the solid blue rectangles, which are separated by the chargon gap 2Δ. With finite mean-field coupling u, the hybridization between the CB and the chargons mix the states, so the CB has a fraction of states at the energies of chargon bands, denoted by the blue dashed rectangles. Meanwhile, the hybridized chargons have states at the energy levels of the CB, denoted by the green dashed lines. (c) The impurity electronic DOS diagram. The magnetic impurity has the original atomic energy levels at $\omega = \epsilon_0 \pm \frac{U}{2}$, which give the peaks in the solid spectrum. With finite coupling to a $U(1)$ QSL with SFS, there emerge new states at the Hubbard band energies denoted by the dashed spectrum. (d) The resonance peak at the Fermi energy in the SAF spectral function $\rho_{a,\sigma}(\omega)$. The inset shows that the local spin at the impurity is screened by the spinon Kondo cloud, which is shown in gold. (e) The CB spectral function $\rho_{X_d}(\omega)$. (f) The impurity bare electronic spectral function $\rho^0_{d,\sigma}(\omega)$, before spinon-chargon binding is taken into account. The spectral functions in (d), (e), and (f) are numerically calculated for a magnetic impurity on a QSL of triangular lattice.

with the effective broadening function defined as $\Gamma_{\text{eff}} = \frac{\pi w^2}{2\Lambda_f}$. The detailed derivation about the two algebra equations are present in Appendix B. The electronic coupling V_R thereby determines the mean-field couplings w and u in the SAF spinon channel and the CB chargon channel, respectively.

In the coupling channel of the SAF and spinon, now the finite mean-field coupling w allows an auxiliary fermion at the impurity to have spin exchange with the itinerant spinons in the $U(1)$ QSL, as is shown in Fig. 2(a). Near the impurity, itinerant spinons at the Fermi level get spin flip scattered by the local magnetic moment, and the local spin at the impurity is also coherently switched in the scattering process. This magnetic scattering yields resonance at the impurity. In the presence of finite coupling to the itinerant spinons, the Matsubara Green's function for the SAF at the impurity is modified to be $G_{a,\sigma}(i\omega_n) = \frac{1}{i\omega_n - i\Gamma_{\text{eff}}}$, so the SAF spectral function $\rho_{a,\sigma}(\omega) = \frac{1}{\pi}\frac{\Gamma_{\text{eff}}}{\omega^2 + \Gamma_{\text{eff}}^2}$ always shows a resonance at the Fermi energy. This is the Kondo-like resonance in the spinon channel. The width of the resonance is solved to be $\Gamma_{\text{eff}} = \Lambda_f \exp(-\frac{U\Lambda_f}{4V_R^2})$, which denotes the Kondo temperature energy scale $k_b T_K$, same as that in a metallic host [2]. Below the Kondo temperature T_K, the nearby spinons of opposite spin are strongly correlated with the local SAF at the impurity, forming the Kondo cloud of size ξ_K [4] to screen the local

magnetic moment, as is shown in the inset in Fig. 2(d). For a magnetic impurity based on a $U(1)$ QSL with SFS, the spinon Kondo resonance and the spinon Kondo screening cloud are in analogy to the conventional Kondo effect of a magnetic impurity in a metal, as in both cases the spin exchange enables the spin fluctuations at the impurity.

The CB chargon coupling channel of the magnetic impurity based on a $U(1)$ QSL, on the other hand, makes the difference from that in the conventional Kondo effect. In the QSL, the chargons are gapped, and the mean-field coupling u enables the hybridization between the chargons and the CB at the impurity. Due to the hybridization, the charged bosonic state at the impurity gets mixed with the chargon states in the QSL, so a fraction of chargon states are transferred to the CB at the impurity, as is schematically shown in Fig. 2(b) by the blue dashed rectangles. The hybridization with the chargons in the QSL modifies the CB Matsubara Green's function to be $G_{X_d}(i\nu_n) \approx \frac{1}{i\nu_n + \epsilon_0 + \frac{U}{2}} - \frac{1}{i\nu_n + \epsilon_0 - \frac{U}{2}} + ZG_X(i\nu_n, \boldsymbol{R}, \boldsymbol{R})$, with $Z = \frac{16u^2 U^2}{(U^2 - 4\epsilon_0^2)^2}$ the spectral weight (see Appendix C for the derivation about the spectral weight), so the CB spectral function $\rho_{X_d}(\omega) = -\frac{1}{\pi}\text{Im}G_{X_d}(i\nu_n \to \omega + i0^+)$ now not only shows the peaks from the original two energy levels, but it also includes a fraction of chargon states at the energy of QSL chargon bands. Differing from the conventional Kondo

effect in a metallic base where the condensed chargons induce the local CB condensation at the impurity [36], the magnetic impurity on $U(1)$ QSL with SFS has the impurity charged bosonic state mixed with a fraction of chargon states in the QSL.

With both channels of the SAF spinon coupling and the CB chargon coupling analyzed, the electronic Matsubara Green's function for the magnetic impurity based on the QSL is ready to be obtained from the convolution in Eq. (11), which yields the form

$$G_{d,\sigma}^0(i\omega_n) \approx \frac{1}{2}\left[\frac{1}{i\omega_n - \epsilon_0 + \frac{U}{2}} + \frac{1}{i\omega_n - \epsilon_0 - \frac{U}{2}} \right.$$
$$\left. + Z\sum_{\mathbf{k}} \left(\frac{1}{i\omega_n + \epsilon_{\mathbf{k}}} + \frac{1}{i\omega_n - \epsilon_{\mathbf{k}}} \right) \right]. \quad (13)$$

The impurity bare electronic spectral function is thus derived to be $\rho_{d,\sigma}^0(\omega) \approx \frac{1}{2}[\delta(\omega - \epsilon_0 + \frac{U}{2}) + \delta(\omega - \epsilon_0 - \frac{U}{2}) + Z|\rho_X(\omega)|]$ with $\rho_X(\omega) = -\frac{1}{\pi}\text{Im}G_X(i\nu_n \to \omega + i0^+, \mathbf{R}, \mathbf{R})$. The calculations of $G_{d,\sigma}^0(i\omega_n)$ and $\rho_{d,\sigma}^0(\omega)$ through convolution are carried out in the spectral representation, which can be found in Eqs. (D6) and (D7) in Appendix D. In addition to the atomic energy level induced peaks at $\omega = \epsilon_0 \pm \frac{U}{2}$, the impurity bare electronic spectral function $\rho_{d,\sigma}^0(\omega)$ now involves the chargon DOS $|\rho_X(\omega)|$ with a spectral weight Z, as the dashed spectrum shows in Fig. 2(c). The peak in the spectrum comes from van Hove singularity in the tight-binding chargon band that we assumed. These impurity states at the energy of chargon bands take a fraction of QSL electronic states transferred through the spinon Kondo resonance in the SAF spinon channel and the hybridization in the CB chargon channel. The magnetic impurity on $U(1)$ QSL with SFS therefore acts as a local probe of the chargon DOS in the QSL.

IV. FULL MEAN-FIELD CALCULATION FOR A MAGNETIC IMPURITY IN A QSL

To verify the above analysis of a magnetic impurity weakly coupled to a $U(1)$ QSL with SFS, the self-consistent equations (5)–(8) are numerically solved in the spectral representation (see Appendix D for the detailed self-consistent integral equations in the spectral representation). With regard to the recent two-dimensional $U(1)$ QSL candidates monolayer TaSe₂ [30–32], which is in a triangular lattice, we take the spinon band dispersion $\xi_{\mathbf{k}}$ and the chargon band dispersion $\epsilon_{\mathbf{k}}$ to be $\xi_{\mathbf{k}} = 2t_f(2\cos\frac{1}{2}k_x a \cos\frac{\sqrt{3}}{2}k_y a + \cos k_x a) - \mu_f$ and $\epsilon_{\mathbf{k}} = 2t_X(2\cos\frac{1}{2}k_x a \cos\frac{\sqrt{3}}{2}k_y a + \cos k_x a - 3) + \Delta$, respectively. Here a is the lattice constant, $t_f = 0.05$ eV is the spinon hopping, $t_X = -0.03$ eV is the chargon hopping, $\mu_f = -0.04$ eV is the spinon chemical potential that makes the spinon band half-filled, and $\Delta = 0.25$ eV is the Mott gap size to match the recent STS measurement on TaSe₂ [32]. The spinon spectral function $\rho_{f,\sigma}(\omega) = -\frac{1}{\pi}\text{Im}\sum_{\mathbf{k}}\frac{1}{\omega + i0^+ - \xi_{\mathbf{k}}}$, the chargon spectral function $\rho_X(\omega) = -\frac{1}{\pi}\text{Im}\sum_{\mathbf{k}}(\frac{1}{\omega + i0^+ + \epsilon_{\mathbf{k}}} - \frac{1}{\omega + i0^+ - \epsilon_{\mathbf{k}}})$, and the convolution generated electronic spectral function $\rho_{c,\sigma}(\omega)$ for the $U(1)$ QSL in a triangular lattice have been calculated and shown in Fig. 4. At the magnetic impurity, we set the impurity on-site energy to be $\epsilon_0 = 0$ eV, which

corresponds to the symmetric Anderson impurity model. The Coulomb repulsion at the impurity is considered to be $U = 3$ eV, which is much larger than the Mott gap Δ, so the atomic energy levels do not have energy overlap with the Hubbard bands in QSL. The full numerical solutions to the self-consistent equations (5)–(8) yield the SAF spinon coupling w and CB chargon coupling u as a function of the electronic coupling V_R, as is shown in Fig. 1(b). The w and u are extremely small at weak coupling V_R, and then they become significantly nonzero as V_R increases. With a given electronic coupling V_R, the nontrivial solutions of w and u from Eqs. (5)–(8) are always guaranteed as long as the on-site interaction U is sufficiently large to induce a local magnetic moment formed at the impurity.

With the self-consistent equations generated mean-field parameters w, u, h, and λ, the SAF spectral function $\rho_{a,\sigma}(\omega) = -\frac{1}{\pi}\text{Im}G_{a,\sigma}(i\omega_n \to \omega + i0^+)$ and the CB spectral function $\rho_{X_d}(\omega) = -\frac{1}{\pi}\text{Im}G_{X_d}(i\nu_n \to \omega + i0^+)$ are numerically calculated and shown in Figs. 2(d) and 2(e). Consistent with our analysis for a magnetic impurity weakly coupled to a $U(1)$ QSL with SFS, the SAF spectral function $\rho_{a,\sigma}(\omega)$ has the spinon Kondo resonance at the Fermi energy, and the CB spectral function $\rho_{X_d}(\omega)$ in the QSL chargon band energy region $-\Lambda_X < \omega < \Lambda_X$ replicates the QSL chargon spectral function $\rho_X(\omega)$ with a spectral weight Z. The original spectral feature of the CB at $\omega = \pm\frac{1}{2}U$ appears as well in the presence of coupling u. Convolving the SAF Green's function $G_{a,\sigma}(i\omega_n \to \omega + i0^+)$ with $G_{X_d}(i\nu_n \to \omega + i0^+)$ then yields the bare electronic spectral function $\rho_{d,\sigma}^0(\omega)$ for the magnetic impurity based on the QSL of a triangular lattice, as is shown in Fig. 2(f). In addition to the peaks from the two atomic energy levels at $\omega = \pm\frac{1}{2}U$, $\rho_{d,\sigma}^0(\omega)$ at $-\Lambda_X < \omega < \Lambda_X$ becomes nonzero and resembles the QSL chargon DOS $|\rho_X(\omega)|$ with a spectral weight. The two peaks shown in $\rho_{d,\sigma}^0(\omega)$ at $-\Lambda_X < \omega < \Lambda_X$ are from the Van Hove singularities of the QSL chargon bands. At the Hubbard band-edge energies $\omega = \pm\Delta$, the impurity bare electronic spectral function $\rho_{d,\sigma}^0(\omega)$ has a step that is inherited from the QSL chargon DOS $|\rho_X(\omega)|$. The bare impurity spectral function $\rho_{d,\sigma}^0(\omega)$ from the full numerical self-consistent calculations again confirm our analysis that the magnetic impurity on $U(1)$ QSL with SFS locally measures the chargon DOS in the QSL.

V. BAND-EDGE RESONANCE PEAKS AND IN-GAP BOUND STATES FROM SPINON-CHARGON BINDING INTERACTION

The step edges of $\rho_{d,\sigma}^0(\omega)$ at the Hubbard band-edge energies $\omega = \pm\Delta$ make the impurity bare electronic states susceptible to the residue spinon-chargon interaction in the QSL host. In the $U(1)$ QSL with SFS, the spinons and chargons both couple to the emergent $U(1)$ gauge field, so the gauge field fluctuations in turn modify the QSL electronic states and further affect the impurity electronic state that couples to electrons in the QSL host. At the Hubbard band-edge energies $\omega = \pm\Delta$, the transverse components of the gauge field fluctuations are neglected here due to the small current-current correlation at band edges, so the longitudinal component of the gauge field fluctuations plays the dominant role [42]. Since the spinons and chargons carry
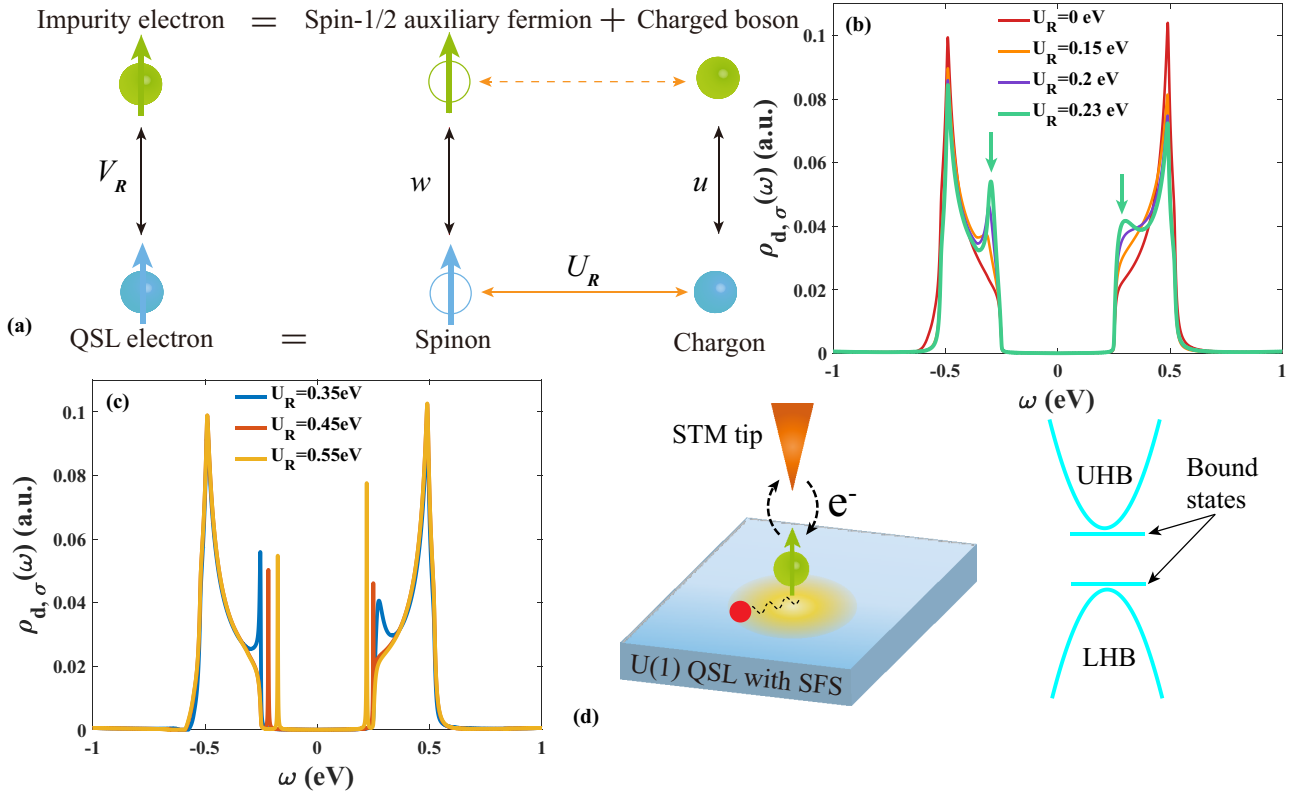
FIG. 3. (a) The schematic diagram showing the spinon-chargon binding interaction incorporated in the slave rotor mean-field description. The impurity electronic state is affected by the spinon-chargon binding interaction in the QSL. (b) The impurity electronic spectral function $\rho_{d,\sigma}(\omega)$. As the spinon-chargon binding interaction in the QSL increases from 0, a pair of resonance peaks emerge at the Hubbard band-edge energies as indicated by the arrows. The original atomic energy levels at $\omega = \pm\frac{U}{2}$ lie outside the range of energies we plot. (c) The in-gap bound state peaks in $\rho_{d,\sigma}(\omega)$. As the binding interaction increases further, the band-edge resonance peaks move inside the Mott gap and evolve to be in-gap bound state peaks. (d) A schematic plot of an STM setup to measure the density of states spectroscopy of the magnetic impurity. The filled red circle with a wavy line connected to the magnetic impurity denotes the hole or electronic state bound to the magnetic impurity. In the negative bias of $\omega \approx -\Delta$, the hole state bound to the magnetic impurity is excited so that an in-gap bound state peak emerges above the top of the LHB. Similarly, a positive bias of $\omega \approx \Delta$ injects an electron into the magnetic impurity and excites the electronic state bound to the magnetic impurity, generating an electronic bound state peak below the UHB bottom.

the opposite gauge charge, the longitudinal component of gauge field fluctuations yields a binding between a spinon and a chargon, which is the spinon-chargon binding interaction [40,41]. In the presence of spinon-chargon binding interaction at the QSL, a spinon tends to get bound with a chargon to form a physical electronic state. At the magnetic impurity, the SAF has spin exchange with the spinon Kondo cloud, and the CB gets hybridized with the nearby chargons, so the spinon-chargon binding interaction in the QSL host affects the impurity electronic state, as is schematically shown in Fig. 3(a).

To take into account the spinon charge binding interaction in the QSL, we notice that the chargons in the QSL are relativistic [34] and contain both holons and doublons: $X_{\boldsymbol{r}} = a_{\boldsymbol{r}} + b_{\boldsymbol{r}}^\dagger$, $X_{\boldsymbol{r}}^\dagger = a_{\boldsymbol{r}}^\dagger + b_{\boldsymbol{r}}$, with the holon annihilation (creation) operator $a_{\boldsymbol{r}}^{(\dagger)}$ and the doublon annihilation (creation) operator $b_{\boldsymbol{r}}^{(\dagger)}$. Assuming a noncompact U(1) gauge field, the fluctuations of the longitudinal component give rise to the spinon-chargon binding interaction term:

$$S' = \int_0^\beta \int \sum_\sigma U_{\boldsymbol{r}} f_{\sigma,\boldsymbol{r}}^\dagger f_{\sigma,\boldsymbol{r}} (a_{\boldsymbol{r}}^\dagger a_{\boldsymbol{r}} - b_{\boldsymbol{r}}^\dagger b_{\boldsymbol{r}}) d\boldsymbol{r} \, d\tau, \qquad (14)$$

where $U_r > 0$ is the spinon-chargon binding interaction strength. The detailed derivation of Eq. (14) can be found in Appendix E. Since the longitudinal interaction is screened by the spinon Fermi sea, we approximate the interaction as short range and on site only. In Appendix E, the binding interaction strength has been estimated to be around half of the spinon bandwidth: $U_r \approx \Lambda_f$. The interaction between a spinon and a doublon in S' is attractive, so a spinon tends to get bound with a doublon to form an electronic bound state. On the other hand, the repulsion between a spinon and a holon in S' manifests the attraction between a spinon hole and a holon, so a spinon hole tends to bind a holon to form a hole bound state. Around a magnetic impurity, the spinon Kondo cloud has both spinon excitations and spinon hole excitations, so in principle both an electronic state and a hole state bound to the magnetic impurity can be induced by a sufficiently large binding interaction.

In the presence of the spinon-chargon binding interaction, the action for a magnetic impurity embedded in a $U(1)$ QSL with SFS becomes $S = S_0 + S'$. At the impurity, the charged bosonic operator can also be written in terms of the holon and doublon operators as $X_d = a_d + b_d^\dagger$, $X_d^\dagger = a_d^\dagger + b_d$, so

the impurity electronic Matsubara Green's function $G_{d,\sigma}(i\omega_n)$ calculates the thermal average from S:

$$G_{d,\sigma}(i\omega_n) = -\int_0^\beta \langle a_\sigma(\tau)a_\sigma^\dagger(0)\rangle[\langle a_d^\dagger(\tau)a_d(0)\rangle$$
$$+ \langle b_d(\tau)b_d^\dagger(0)\rangle]d\tau. \quad (15)$$

Due to the spinon-chargon binding interaction in the QSL, a doublon tends to get bound with a spinon to form an electronic state, and a holon tends to get bound with a spinon hole to form a hole state. It is known that the CB $X_d = a_d + b_d^\dagger$ at the impurity couples to the chargons in the QSL through the mean-field parameter u, and the SAF a_σ at the impurity couples to the spinons in the QSL through the mean-field parameter w, so the impurity electronic Matsubara Green's function can be calculated through the random phase approximation. The resulting impurity electronic Matsubara Green's function $G_{d,\sigma}(i\omega_n)$ takes the form

$$G_{d,\sigma}(i\omega_n) = G_{d,\sigma}^0(i\omega_n) + \sum_{i,j=1,2}\{\hat{T}_\sigma(i\omega_n)U_{\boldsymbol{R}}\sigma_z$$
$$\times [1 - \hat{G}_{c,\sigma}(i\omega_n)U_{\boldsymbol{R}}\sigma_z]^{-1}\hat{T}_\sigma(i\omega_n)\}_{ij}. \quad (16)$$

A detailed derivation of $G_{d,\sigma}(i\omega_n)$ can be found in Appendix F. Here σ_z is the z component of the Pauli matrix acting on the holon and doublon space, and $\hat{T}_\sigma(i\omega_n)$, $\hat{G}_{c,\sigma}(i\omega_n)$ are both 2×2 correlators,

$$\hat{T}_\sigma(i\omega_n) = -\int_0^\beta \langle a_\sigma(\tau)f_{\sigma,\boldsymbol{R}}^\dagger(0)\rangle_0$$
$$\times \left\langle \begin{pmatrix} a_d^\dagger(\tau)a_{\boldsymbol{R}}(0) & a_d^\dagger(\tau)b_{\boldsymbol{R}}^\dagger(0) \\ b_d(\tau)a_{\boldsymbol{R}}(0) & b_d(\tau)b_{\boldsymbol{R}}^\dagger(0) \end{pmatrix} \right\rangle_0 d\tau, \quad (17)$$

$$\hat{G}_{c,\sigma}(i\omega_n) = -\int_0^\beta \langle f_{\sigma,\boldsymbol{R}}(\tau)f_{\sigma,\boldsymbol{R}}^\dagger(0)\rangle_0$$
$$\times \left\langle \begin{pmatrix} a_{\boldsymbol{R}}^\dagger(\tau)a_{\boldsymbol{R}}(0) & a_{\boldsymbol{R}}^\dagger(\tau)b_{\boldsymbol{R}}^\dagger(0) \\ b_{\boldsymbol{R}}(\tau)a_{\boldsymbol{R}}(0) & b_{\boldsymbol{R}}(\tau)b_{\boldsymbol{R}}^\dagger(0) \end{pmatrix} \right\rangle_0 d\tau, \quad (18)$$

with $\langle\cdots\rangle_0$ being the thermal average calculated from S_0 in Eq. (4). The more detailed forms of $\hat{T}_\sigma(i\omega_n)$ and $\hat{G}_{c,\sigma}(i\omega_n)$ have been derived in Appendix F. The spinon-chargon binding interaction $U_{\boldsymbol{R}}$ in the QSL modifies the impurity electronic Green's function through the second term in Eq. (16).

As the spinon-chargon binding interaction increases from 0, it induces the spectral weight to transfer from the bulk Hubbard bands to the band edges. At $U_{\boldsymbol{R}} = 0.23$ eV, which is around half of the spinon bandwidth we considered (see Fig. 4 in Appendix E), a pair of band-edge resonance peaks arise, as seen in Fig. 3(b). The band-edge resonance peaks indicated by the arrows in Fig. 3(b) are still located inside the Hubbard bands, so the band-edge resonance peaks have the intrinsic width that is determined by the spinons, chargons, and their coupling to the impurity electronic state. Importantly, the band-edge resonance peaks appear only at the magnetic impurity but do not show up in the pristine QSL given the same binding interaction (see Fig. 5 in Appendix F for comparison). Such band-edge resonance peaks at the Hubbard band edges can be regarded as the precursors to in-gap bound states.

As the spinon-chargon binding interaction increases further, the band-edge resonance peaks gradually move inside the Mott gap and develop into in-gap peaks of bound states, as is shown in Fig. 3(c). The in-gap bound states arise from the new poles of $G_{d,\sigma}(i\omega_n \rightarrow \omega + i0^+)$ that come from $U_{\boldsymbol{R}}\sigma_z[1 - \hat{G}_{c,\sigma}(i\omega_n \rightarrow \omega + i0^+)U_{\boldsymbol{R}}\sigma_z]^{-1}$ at a sufficiently large binding $U_{\boldsymbol{R}}$, so an electronic bound state and a hole bound state appear below the UHB bottom and above the LHB top, respectively, as shown in Figs. 3(c) and 3(d). The in-gap peaks of the bound states have no intrinsic width, so we introduce an extrinsic broadening of 5 meV to make them better visualized in Fig. 3(c).

Physically, the band-edge resonance peaks in the magnetic impurity spectral function $\rho_{d,\sigma}(\omega)$ near $\omega \approx \pm\Delta$ and the in-gap peaks of the bound states can be interpreted as the joint effect of the spinon Kondo screening cloud and the spinon-chargon binding interaction around the magnetic impurity. At the top of the LHB, a spinon hole excitation in the spinon Kondo cloud attracts a holon to form a hole excitation. The hole excitation is manifested as a band-edge resonance peak at a moderate binding interaction, and it evolves into an in-gap hole bound state as the binding interaction increases further. In analogy to an acceptor impurity embedded in a semiconductor, the hole excitation and its descendent hole bound state around the magnetic impurity appear at the top of the LHB, as seen in Figs. 3(b)–3(d). At the bottom of the UHB, the attraction between a spinon in the spinon Kondo cloud and a doublon gives rise to an electronic excitation, which also shows up as a band-edge resonance peak in $\rho_{d,\sigma}(\omega)$. As the binding interaction increases, the band-edge resonance peak moves down into the Mott gap and develops into an in-gap electronic bound state peak. Similar to a donor impurity in a semiconductor, the electronic excitation and the descendent in-gap electronic bound state around the magnetic impurity form at the bottom of the UHB, as shown in Figs. 3(b)–3(d). When a scanning tunneling microscope (STM) tip is put on top of the magnetic impurity, as seen in Fig. 3(d), applying a negative bias with $\omega \approx -\Delta$ extracts an electron out of the QSL and creates a hole near the magnetic impurity. Depending on the binding interaction strength, either a band-edge resonance peak at the LHB top or a hole bound state peak above the LHB top appears. On the other hand, applying a positive bias with $\omega \approx \Delta$ injects an electron into the QSL through the magnetic impurity, which induces either a band-edge resonance peak at the UHB bottom or an electronic bound state peak below the UHB bottom, depending on the binding interaction strength. Since the spinon Kondo screening cloud has both the spinon hole excitations attractive to the holons and the spinon excitations attractive to the doublons, the magnetic impurity screened by the spinon cloud acts as an impurity of acceptor and donor type simultaneously, generating a peak located at the top of the UHB and one at the bottom of the LHB. Such a spectral feature induced by a magnetic impurity embedded in a Mott insulator therefore indicates that the host Mott insulator is a $U(1)$ QSL with SFS. Since the effective attraction comes from the longitudinal component of gauge field fluctuations, the peaks near $\omega \approx \pm\Delta$ in the spectroscopy of a magnetic impurity manifest the gauge field fluctuations in the $U(1)$ QSL with SFS.

VI. CONCLUSION AND DISCUSSIONS

In the above sections, applying the slave rotor mean-field theory and incorporating the longitudinal component of gauge field fluctuations, the electronic spectral function of a magnetic impurity embedded in a $U(1)$ QSL with SFS was calculated. At the mean-field level where the gauge field fluctuations are neglected in the QSL, the magnetic impurity has the spinon Kondo screening cloud around and locally measures the chargon DOS in the QSL. When the gauge field fluctuations are included in the QSL, the resulting spinon chargon binding interaction in the spinon Kondo cloud induces a pile-up of spectral weight at the Hubbard band edges, which shows up as band-edge resonance peaks in the spectroscopy of the magnetic impurity. The band-edge resonance peaks appear due to the joint effect of the spinon Kondo cloud and the gauge field fluctuations at the QSL sites around the magnetic impurity. As a result, in the spectroscopy of a magnetic impurity, a pair of resonance peaks emerging at $\omega \approx \pm\Delta$ of the Hubbard band edges provide strong evidence that the host Mott insulator is a $U(1)$ QSL with SFS.

Recently, scanning tunneling spectroscopy measurements have been carried out on a Co adatom embedded in a monolayer TaSe$_2$ [32], which is a QSL candidate. The spectroscopy measurements on top of the Co adatom exhibit a resonance peak at both the LHB top and UHB bottom, while a contrast measurement on an Au impurity shows no resonance peaks. As the Co atom carries a local magnetic moment, it matches our theory of a magnetic impurity embedded on a $U(1)$ QSL with SFS. Based on our theory, the observation of the resonance peaks in the spectroscopy of a Co adatom strongly suggests that the monolayer Mott insulator TaSe$_2$ has the spinon Fermi surface and emergent $U(1)$ gauge field.

Our establishment of the spectral function for a magnetic impurity on $U(1)$ QSL with SFS suggests that depositing a magnetic impurity on a Mott insulator and carrying out spectroscopy measurements on the impurity can serve as a diagnosis for the QSL state. Recently new two-dimensional electronic correlation-induced insulators emerged with moiré flat bands [43–45], thus the magnetic impurity deposit followed by spectroscopy measurements is expected to identify more candidates for $U(1)$ QSL with SFS.

APPENDIX A: SPECTRAL REPRESENTATION OF A GREEN'S FUNCTION

We first review the spectral representation of a Green's function. For a Green's function $\mathcal{G}(z)$, its spectral representation reads

$$\mathcal{G}(z) = -\int_{-\infty}^{\infty} \frac{\text{Im}\mathcal{G}(\omega' + i0^+)}{z - \omega} \frac{d\omega'}{\pi}. \tag{A1}$$

Here z is complex. When z takes $z = i\omega_n$ or $z = i\nu_n$, the Green's function $\mathcal{G}(z)$ is a Matsubara Green's function. When z takes $z = \omega + i0^+$, the Green's function $\mathcal{G}(z)$ is a retarded Green's function. The spectral representation of the Green's function is widely used in our calculations.

For the $U(1)$ QSL with SFS, its on-site spinon Matsubara Green's function takes the form

$$G_{f,\sigma}(i\omega_n, \boldsymbol{R}, \boldsymbol{R}) = -\langle f_{\sigma,\boldsymbol{R}}(i\omega_n)f^\dagger_{\sigma,\boldsymbol{R}}(i\omega_n)\rangle_0 e^{i(\boldsymbol{k}-\boldsymbol{k}')\cdot\boldsymbol{R}}$$
$$= \frac{1}{\Omega}\sum_{\boldsymbol{k}} \frac{1}{i\omega_n - \xi_{\boldsymbol{k}}}, \tag{A2}$$

with Ω the volume of the system. The spinon Matsubara Green's function can also be expressed in the spectral representation as

$$G_{f,\sigma}(i\omega_n, \boldsymbol{R}, \boldsymbol{R}) = \int_{-\infty}^{\infty} \frac{\rho_{f,\sigma}(\omega')}{i\omega_n - \omega'}d\omega', \tag{A3}$$

with the spinon spectral function $\rho_{f,\sigma}(\omega') = -\frac{1}{\pi}\text{Im}G^R_{f,\sigma}(\omega')$ and $G^R_{f,\sigma}(\omega') = G_{f,\sigma}(i\omega_n \to \omega' + i0^+)$. Similarly, the on-site chargon Green's function can be written as

$$G_X(i\nu_n, \boldsymbol{R}, \boldsymbol{R}) = \langle X_{\boldsymbol{R}}(i\nu_n)X^\dagger_{\boldsymbol{R}}(i\nu_n)\rangle_0$$
$$= \frac{1}{\Omega}\sum_{\boldsymbol{k}} \left(\frac{1}{i\nu_n + \epsilon_{\boldsymbol{k}}} - \frac{1}{i\nu_n - \epsilon_{\boldsymbol{k}}}\right), \tag{A4}$$

and its spectral representation reads

$$G_X(i\nu_n, \boldsymbol{R}, \boldsymbol{R}) = \int_{-\infty}^{\infty} \frac{\rho_X(\omega')}{i\nu_n - \omega'}d\omega', \tag{A5}$$

with the chargon spectral function $\rho_X(\omega') = -\frac{1}{\pi}\text{Im}G^R_X(\omega')$ and $G^R_X(\omega') = G_X(i\nu_n \to \omega' + i0^+)$.

APPENDIX B: DERIVATION OF THE TWO APPROXIMATED ALGEBRA EQUATIONS

In the isolated magnetic impurity with zero coupling, the SAF has the bare Matsubara Green's function $G^0_{a,\sigma}(i\omega_n) = \frac{1}{i\omega_n}$, and the CB has the bare Matsubara Green's function $G^0_{X_d}(i\nu_n) = \frac{1}{i\nu_n + \epsilon_0 + \frac{U}{2}} - \frac{1}{i\nu_n + \epsilon_0 - \frac{U}{2}}$ [35].

In the magnetic impurity weakly coupled to the $U(1)$ QSL with SFS, by taking the approximated Lagrangian multipliers to be $h = \epsilon_0$, $\lambda = \frac{U}{4} - \frac{h^2}{U}$, the Matsubara frequency summation in Eq. (5) can be calculated as

$$\frac{1}{\beta}\sum_{\omega_n} G_{a,\sigma}(i\omega_n)G_{f,\sigma}(i\omega_n, \boldsymbol{R}, \boldsymbol{R})$$
$$= -\frac{1}{\pi}\int_{-\infty}^{\infty} \text{Im}\frac{G^R_1(\omega)}{1 - w^2 G^R_1(\omega)}n_F(\omega)d\omega$$
$$\approx -\frac{1}{\pi}\int_{-\infty}^{0} \frac{\text{Im}G^R_1(\omega)}{1 + \left[w^2\text{Im}G^R_1(\omega)\right]^2}d\omega, \tag{B1}$$

with

$$G_1^R(\omega) = G_{a,\sigma}^0(i\omega_n \to \omega + i0^+)G_{f,\sigma}(i\omega_n \to \omega + i0^+, \mathbf{R}, \mathbf{R})$$

$$= \frac{1}{\omega + i0^+}\left[\int_{-\infty}^{\infty}\frac{\rho_{f,\sigma}(\omega')}{\omega - \omega'}d\omega' - i\pi\rho_{f,\sigma}(\omega)\right], \quad \text{(B2)}$$

and the Fermi distribution function $n_F(\omega) = \frac{1}{e^{\beta\omega}+1}$. For simplicity, the spinon DOS is assumed to be constant, $\rho_{f,\sigma}(\omega) = \frac{1}{2\Lambda_f}\Theta(\Lambda_f^2 - \omega^2)$, and the self-consistent equation (5) is simplified to be

$$u \approx -2wV_{\mathbf{R}}\int_{-\Lambda_f}^0\frac{\omega}{\omega^2 + \Gamma_{\text{eff}}^2}\frac{1}{2\Lambda_f}d\omega = -\frac{wV_{\mathbf{R}}}{2\Lambda_f}\ln\frac{\Gamma_{\text{eff}}^2}{\Lambda_f^2 + \Gamma_{\text{eff}}^2},$$
$$\text{(B3)}$$

with $\Gamma_{\text{eff}} = \frac{\pi w^2}{2\Lambda_f}$. In Eq. (6), the Matsubara frequency summation can be calculated as

$$\frac{1}{\beta}\sum_{\nu_n}G_{X_d}(i\nu_n)G_X(i\nu_n, \mathbf{R}, \mathbf{R})$$

$$= \frac{1}{\pi}\int_{-\infty}^{\infty}\text{Im}\frac{G_2^R(\omega)}{1 - u^2 G_2^R(\omega)}n_B(\omega)d\omega$$

$$\approx -\frac{1}{\pi}\int_{-\infty}^{\infty}\frac{\text{Im}G_2^R(\omega)}{1 + [u^2\text{Im}G_2^R(\omega)]^2}d\omega, \quad \text{(B4)}$$

with

$$G_2^R(\omega) = G_{X_d}^0(i\nu_n \to \omega + i0^+)G_X(i\nu_n \to \omega + i0^+, \mathbf{R}, \mathbf{R})$$

$$\approx \frac{4U}{U^2 - 4\epsilon_0^2}\left[\int_{-\infty}^{\infty}\frac{\rho_X(\omega')}{\omega - \omega'}d\omega' - i\pi\rho_X(\omega)\right], \quad \text{(B5)}$$

and the Bose distribution function $n_B(\omega) = \frac{1}{e^{\beta\omega}-1}$. For simplicity, the chargon DOS is assumed to be constant: $\rho_X(\omega) = \frac{1}{\Lambda_X - \Delta}$ for $-\Lambda_X < \omega < -\Delta$ and $\rho_X(\omega) = -\frac{1}{\Lambda_X - \Delta}$ for $\Delta < \omega < \Lambda_X$. Then the self-consistent equation in Eq. (6) is simplified to be

$$w = uV_{\mathbf{R}}\int_{-\Lambda_X}^{-\Delta}\frac{\frac{4U}{U^2 - 4\epsilon_0^2}\frac{1}{\Lambda_X - \Delta}}{1 + \left[\frac{4\pi u^2 U}{(U^2 - 4\epsilon_0^2)(\Lambda_X - \Delta)}\right]^2}d\omega \approx \frac{4uUV_{\mathbf{R}}}{U^2 - 4\epsilon_0^2}. \quad \text{(B6)}$$

In a magnetic impurity weakly coupled to a $U(1)$ QSL with SFS, the mean-field self-consistent equations (5) and (6) are then approximated by the two algebra equations (B3) and (B6), respectively.

APPENDIX C: DERIVATION OF THE SPECTRAL WEIGHT

In the presence of mean-field coupling u, the CB Matsubara Green's function in Eq. (10) can be approximated by the Dyson equation as

$$G_{X_d}(i\nu_n) = \frac{G_{X_d}^0(i\nu_n)}{1 - u^2 G_{X_d}^0(i\nu_n)G_X(i\nu_n, \mathbf{R}, \mathbf{R})}$$

$$\approx G_{X_d}^0(i\nu_n)\left[1 + u^2 G_X(i\nu_n, \mathbf{R}, \mathbf{R})G_{X_d}^0(i\nu_n)\right]. \quad \text{(C1)}$$

As the Coulomb repulsion U is much larger than the low-energy region with which we are concerned, the $G_{X_d}^0(i\nu_n)$ in

the second term is approximated to be $G_{X_d}^0(i\nu_n) \approx \frac{4U}{U^2 - 4\epsilon_0^2}$ and it yields

$$G_{X_d}(i\nu_n) \approx G_{X_d}^0(i\nu_n) + Z\sum_{\mathbf{k}}G_X(i\nu_n, \mathbf{R}, \mathbf{R}). \quad \text{(C2)}$$

Here Z is the spectral weight, which takes the value $Z = \frac{16u^2U^2}{(U^2 - 4\epsilon_0^2)^2}$.

APPENDIX D: SELF-CONSISTENT EQUATIONS IN THE SPECTRAL REPRESENTATION

By taking the spectral representation of Matsubara Green's functions, the self-consistent equations (5)–(8) that involve the infinite summation series can all be written in integral equations form as

$$u = -2wV_{\mathbf{R}}\int_{-\infty}^{\infty}\left[\rho_{a,\sigma}(\omega)\text{Re}G_{f,\sigma}^R(\omega, \mathbf{R}, \mathbf{R})\right.$$
$$\left. + \text{Re}G_{a,\sigma}^R(\omega)\rho_{f,\sigma}(\omega)\right]n_F(\omega)d\omega, \quad \text{(D1)}$$

$$w = -uV_{\mathbf{R}}\int_{-\infty}^{\infty}\left[\rho_{X_d}(\omega)\text{Re}G_X^R(\omega, \mathbf{R}, \mathbf{R})\right.$$
$$\left. + \rho_X(\omega)\text{Re}G_{X_d}^R(\omega)\right]n_B(\omega)d\omega, \quad \text{(D2)}$$

$$1 = -\int_{-\infty}^{\infty}\rho_{X_d}(\omega)n_B(\omega)d\omega, \quad \text{(D3)}$$

$$\int_{-\infty}^{\infty}\rho_{a,\sigma}(\omega)n_F(\omega)d\omega$$

$$= \frac{1}{2} - \frac{h}{U} + \frac{1}{2U}\int_{-\infty}^{\infty}\omega\rho_{X_d}(\omega)\coth\frac{1}{2}\beta\omega d\omega$$

$$- \frac{1}{U\beta}\int_{-\infty}^{\infty}\rho_{X_d}(\omega)d\omega, \quad \text{(D4)}$$

where the superscript R denotes the retarded Green's function obtained by the analytic continuation $i\omega_n \to \omega + i0^+$, $i\nu_n \to \omega + i0^+$ in the corresponding Matsubara Green's function.

In the numerical calculation, the spinon spectral function $\rho_{f,\sigma}(\omega)$ and the chargon spectral function $\rho_X(\omega)$ we considered are plotted in Figs. 4(a) and 4(b), respectively. The resulting electronic spectral function $\rho_{c,\sigma}(\omega)$ can be obtained through the convolution in the spectral representation,

$$\rho_{c,\sigma}(\omega) = \int_{-\infty}^{\infty}\rho_{f,\sigma}(\omega + \omega')\rho_X(\omega')[n_F(-\omega - \omega')$$
$$+ n_B(-\omega')]d\omega', \quad \text{(D5)}$$

and it is plotted in Fig. 4(c).

With a given spinon and chargon Green's function in the host system, the four integral equations can be numerically solved and yield the mean-field parameters w, u, λ, h. In the spectral representation, the convolution of the impurity bare electronic Matsubara Green's function is calculated as

$$G_{d,\sigma}^0(i\omega_n) = \frac{1}{\beta}\sum_{\nu_n}\int_{-\infty}^{\infty}\frac{\rho_{a,\sigma}(\omega')}{i\omega_n + i\nu_n - \omega'}d\omega'\int_{-\infty}^{\infty}\frac{\rho_{X_d}(\nu')}{i\nu_n - \nu'}d\nu'. \quad \text{(D6)}$$
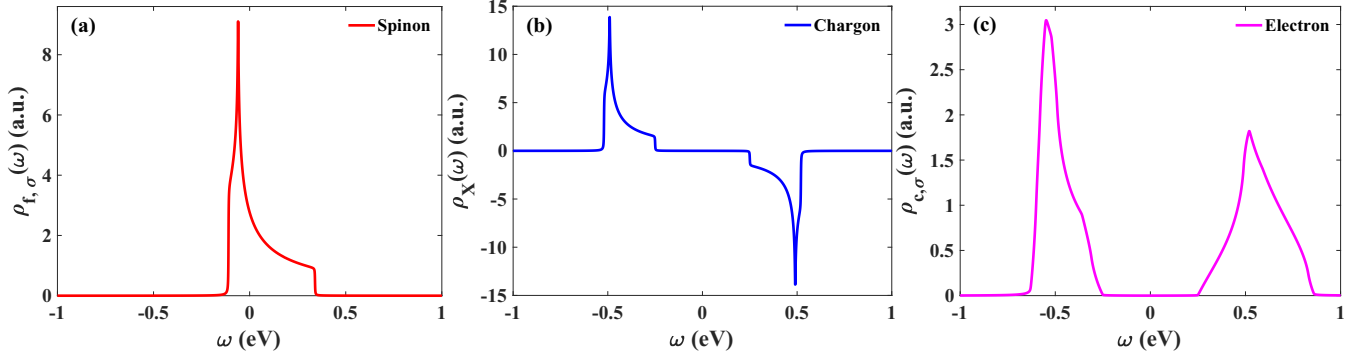
FIG. 4. (a) The spectral function $\rho_{f,\sigma}(\omega)$ for the itinerant spinons in the QSL. (b) The spectral function $\rho_X(\omega)$ for the QSL chargons. (c) The electronic spectral function $\rho_{c,\sigma}(\omega)$ for the $U(1)$ QSL with SFS. The QSL considered here is of a triangular lattice.

By summing over the Matsubara frequency ν_n, the retarded Green's function $G^0_{d,\sigma}(i\omega_n \to \omega + i0^+)$ can be obtained through the analytic continuation. The impurity bare electronic spectral function $\rho^0_{d,\sigma}(\omega) = -\frac{1}{\pi}\text{Im}G^0_{d,\sigma}(i\omega_n \to \omega + i0^+)$ then takes the form

$$\rho^0_{d,\sigma}(\omega) = \int_{-\infty}^{\infty} \rho_{a,\sigma}(\omega + \omega')\rho_{X_d}(\omega')[n_F(-\omega - \omega')$$
$$+ n_B(-\omega')]d\omega'. \tag{D7}$$

APPENDIX E: SPINON-CHARGON BINDING INTERACTION FROM LONGITUDINAL GAUGE FIELD FLUCTUATIONS

The low-energy effective action for the $U(1)$ QSL with SFS is [46]

$$S_{SL} = S_f + S_\phi + S_M, \tag{E1}$$

with the spinon field action

$$S_f = \int_0^\beta d\tau \int d\boldsymbol{r} \sum_\sigma \left[f^\dagger_{\sigma,r}(\partial_\tau + iA_{0,r} - \mu_f)f_{\sigma,r} \right.$$
$$\left. + \frac{\hbar^2}{2m_f}(\partial_r + iA_r)f^\dagger_{\sigma,r} \cdot (\partial_r - iA_r)f_{\sigma,r} \right], \tag{E2}$$

the complex bosonic field action

$$S_\phi = \int_0^\beta d\tau \int d\boldsymbol{r}[(\partial_\tau - iA_{0,r})\phi^\dagger_r(\partial_\tau + iA_{0,r})\phi_r$$
$$+ \hbar^2 v_b^2(\partial_\tau + iA_r)\phi^\dagger_r(\partial_\tau - iA_r)\phi_r + \Delta^2 \phi^\dagger_r \phi_r], \tag{E3}$$

and the Maxwell term that controls the gauge field fluctuations

$$S_M = \frac{1}{2g^2}\int_0^\beta d\tau \int d\boldsymbol{r}[(\nabla A_{0,r} + \partial_\tau A_r)^2 + (\nabla \times A_r)^2]. \tag{E4}$$

Here m_f is the effective spinon mass, v_b is the boson velocity, Δ is the chargon gap, g is the bare gauge field coupling constant, and $A_{0,r}$, A_r are the temporary and spatial components of the $U(1)$ gauge field, respectively. The action S_{SL} is invariant under the local $U(1)$ gauge transformation [34]. At the mean-field level where gauge fields are neglected, the spinon correlation function is $-\langle f_{\sigma,k}(i\omega_n)f^\dagger_{\sigma,k}(i\omega_n)\rangle_0 = \frac{1}{i\omega_n - \xi_k}$ with

$\xi_k = \frac{\hbar^2 k^2}{2m_f} - \mu_f$ the band dispersion in the continuum limit. The chargon operator becomes $X_k^{(\dagger)} = \sqrt{2\epsilon_k}\phi_k^{(\dagger)}$ and the chargon correlation function reads $\langle X_k(i\nu_n)X_k^\dagger(i\nu_n)\rangle_0 = \frac{1}{i\nu_n + \epsilon_k} - \frac{1}{i\nu_n - \epsilon_k}$ with $\epsilon_k = \sqrt{\hbar^2 v_b^2 k^2 + \Delta^2}$ the chargon band dispersion in the continuum limit. When the QSL is considered in a periodic lattice, tight-binding band dispersions ξ_k and ϵ_k can be constructed to replace those in the continuum limit.

In the Coulomb gauge $\nabla \cdot A_r = 0$, as the group velocity at the Hubbard band-edge energies is negligible, the coupling of the transverse gauge field to the current is small, and we drop the transverse gauge field fluctuations. The longitudinal component of gauge field $A_{0,r}$ is kept in S_f, S_ϕ, and S_M. The spinon field action S_f describes the Schrödinger field, but the complex bosonic field S_ϕ describes the Klein-Gordon field. The Klein-Gordon field action S_ϕ can be rewritten in terms of the canonical momentum operators as

$$S_\phi = \int_0^\beta \int d\boldsymbol{r}[\Pi^\dagger_r \partial_\tau \phi^\dagger_r + \Pi_r \partial_\tau \phi_r - iA_{0,r}(\Pi^\dagger_r \phi^\dagger_r - \Pi_r \phi_r)$$
$$- \Pi^\dagger_r \Pi_r + \hbar^2 v_b^2 \partial_r \phi^\dagger_r \partial_r \phi_r + \Delta^2 \phi^\dagger_r \phi_r], \tag{E5}$$

with $\Pi^\dagger_r = (\partial_\tau + iA_{0,r})\phi_r$ and $\Pi_r = (\partial_\tau - iA_{0,r})\phi^\dagger_r$ the canonical momentum operators. We apply the Fourier transformation to Eq. (E5). By introducing new bosonic operators

$$a_k = \frac{1}{2}X_k - \frac{1}{\sqrt{2\epsilon_k}}\Pi^\dagger_k, \quad a^\dagger_k = \frac{1}{2}X^\dagger_k + \frac{1}{\sqrt{2\epsilon_k}}\Pi_k, \tag{E6}$$

$$b_k = \frac{1}{2}X^\dagger_k - \frac{1}{\sqrt{2\epsilon_k}}\Pi_k, \quad b^\dagger_k = \frac{1}{2}X_k + \frac{1}{\sqrt{2\epsilon_k}}\Pi^\dagger_k, \tag{E7}$$

we transform the relativistic Klein-Gordon action to the nonrelativistic Schrödinger type,

$$S_\phi = \int_0^\beta \sum_{k,q}[a_k(-\partial_\tau \delta_{k,q} + iA_{0,-k+q})a^\dagger_q + b^\dagger_k(\partial_\tau \delta_{k,q}$$
$$- iA_{0,-k+q})b_q + \epsilon_k(a_k a^\dagger_k + b^\dagger_k b_k)]. \tag{E8}$$

Importantly, here $a_k^{(\dagger)}$ is the holon operator and $b_k^{(\dagger)}$ is the doublon operator. The doublon and holon together compose the relativistic chargon $X_r = a_r + b_r^\dagger$, $X_r^\dagger = a_r^\dagger + b_r$.

Now with only the longitudinal gauge field, the $U(1)$ QSL with SFS action S_{SL} takes the form

$$S_{SL} = \int_0^\beta d\tau \sum_{\sigma,k,q} \left[f_{\sigma,k}^\dagger(\partial_\tau + \xi_k)f_{\sigma,k} + a_k(-\partial_\tau + \epsilon_k)a_k^\dagger \right.$$
$$+ b_k^\dagger(\partial_\tau + \epsilon_k)b_k + if_{\sigma,k}^\dagger A_{0,k-q}f_{\sigma,q} + ia_k A_{0,-k+q}a_q^\dagger$$
$$\left. - ib_k^\dagger A_{0,-k+q}b_q + \frac{q^2}{2g^2\Omega}A_{0,-q}A_{0,q} \right]. \quad (E9)$$

Integrating out the longitudinal gauge field $A_{0,r}$ then yields the gauge field $A_{0,r}$ fluctuation-induced interaction terms

$$\frac{1}{2}\int dr \int dr' U_{r-r'}^C \sum_{\sigma,\sigma'} [f_{\sigma,r}^\dagger f_{\sigma,r} f_{\sigma',r'}^\dagger f_{\sigma',r'} + (a_r^\dagger a_r$$
$$- b_r^\dagger b_r)(a_{r'}^\dagger a_{r'} - b_{r'}^\dagger b_{r'}) + 2f_{\sigma,r}^\dagger f_{\sigma,r}(a_{r'}^\dagger a_{r'} - b_{r'}^\dagger b_{r'})], \quad (E10)$$

where the Coulomb-type interaction $U_{r-r'}^C = \frac{g^2}{(2\pi)^2}\int \frac{e^{iq\cdot(r-r')}}{q^2+K^2}dq$ has the screening K due to the itinerant spinons [47]. The interaction arising from longitudinal gauge field fluctuations includes the spinon-spinon interaction, the chargon-chargon interaction, and the spinon-chargon binding interaction. The spinon-spinon interaction and the chargon-chargon interaction modify the spinon and chargon correlation function, respectively, but the last term, namely the spinon-chargon binding interaction, tends to bind the spinon and the chargon into an electron, which becomes the dominant effect of the gauge field fluctuations [42].

Taking into account the dominant effect of the gauge field fluctuations, we arrive at the QSL action in the presence of longitudinal gauge field fluctuations,

$$S_{SL} \approx \int_0^\beta d\tau \sum_{\sigma,k} \left[f_{\sigma,k}^\dagger(\partial_\tau + \xi_k)f_{\sigma,k} + a_k(-\partial_\tau + \epsilon_k)a_k^\dagger \right.$$
$$\left. + b_k^\dagger(\partial_\tau + \epsilon_k)b_k + \int U_r f_{\sigma,r}^\dagger f_{\sigma,r}(a_r^\dagger a_r - b_r^\dagger b_r)dr \right]. \quad (E11)$$

Here, we only consider the on-site spinon chargon binding interaction since the screening from the itinerant spinons makes the interaction short-ranged. We know that the Thomas-Fermi screening is $K = g\sqrt{N_f}$, with N_f being the spinon DOS at the Fermi energy, so at $q \to 0$ the spinon chargon binding interaction strength is approximated as

$$U_r \approx \frac{g^2}{(2\pi)^2}\int \frac{1}{g^2 N_f}dq = \int \frac{dq}{4\pi^2 N_f} \approx \Lambda_f. \quad (E12)$$

Here Λ_f is half of the spinon bandwidth. It indicates that the spinon-chargon binding interaction U_r is estimated to be half of the spinon bandwidth.

APPENDIX F: DERIVATION OF THE GAUGE FIELD FLUCTUATION MODIFIED IMPURITY ELECTRONIC GREEN'S FUNCTION

By numerically solving the self-consistent equations (D1)–(D4), we can obtain the SAF spionon coupling w, the CB chargon coupling u, and the Lagrangian multipliers λ, h, so the magnetic impurity on the $U(1)$ QSL with SFS has the quadratic action at the mean-field level,

$$S_0 = \int_0^\beta \sum_\sigma [a_\sigma^\dagger(\partial_\tau + \epsilon_0 - h)a_\sigma + w(f_{\sigma,R}^\dagger a_\sigma + a_\sigma^\dagger f_{\sigma,R})]d\tau$$

$$+ \int_0^\beta \left[\frac{1}{U}(\partial_\tau + h)X_d^\dagger(\partial_\tau - h)X_d + \left(\lambda + \frac{h^2}{U}\right)X_d^\dagger X_d - u(X_d^\dagger X_R + X_R^\dagger X_d) \right]d\tau$$

$$- \int_0^\beta d\tau \int_0^\beta d\tau' \sum_\sigma [f_{\sigma,R}^\dagger(\tau)G_{f,\sigma}^{-1}(\tau,\tau',R,R)f_{\sigma,R}(\tau') - X_R^\dagger(\tau)G_X^{-1}(\tau,\tau',R,R)X_R(\tau')]. \quad (F1)$$

To incorporate the spinon-chargon binding interaction in the QSL into the mean-field action S_0, the holon and doublon operators at the impurity are defined as

$$a_d = \frac{1}{2}\left(X_d - \frac{U}{\sqrt{\lambda U + h^2}}\Pi_d^\dagger\right), \quad (F2)$$

$$a_d^\dagger = \frac{1}{2}\left(X_d^\dagger + \frac{U}{\sqrt{\lambda U + h^2}}\Pi_d\right), \quad (F3)$$

$$b_d = \frac{1}{2}\left(X_d^\dagger - \frac{U}{\sqrt{\lambda U + h^2}}\Pi_d\right), \quad (F4)$$

$$b_d^\dagger = \frac{1}{2}\left(X_d + \frac{U}{\sqrt{\lambda U + h^2}}\Pi_d^\dagger\right), \quad (F5)$$

with the canonical momentum operators defined to be

$$\Pi_d^\dagger = \frac{(\partial_\tau - h)X_d}{U}, \quad \Pi_d = \frac{(\partial_\tau + h)X_d^\dagger}{U}. \quad \text{(F6)}$$

In this way, the CB at the impurity, which is also relativistic, is expressed by the impurity holon and doublon operators as $X_d = a_d + b_d^\dagger$, $X_d^\dagger = a_d^\dagger + b_d$. Therefore, the relativistic-type Klein-Gordon field action at the impurity can also be transformed to the Schrödinger field type.

In the Matsubara frequency space, the Green's functions for the holon and doublon in the QSL are

$$G_a(iv_n, \boldsymbol{R}, \boldsymbol{R}) = \sum_k \frac{1}{iv_n - \epsilon_k}, \quad \text{(F7)}$$

$$G_b(iv_n, \boldsymbol{R}, \boldsymbol{R}) = \sum_k \frac{-1}{iv_n + \epsilon_k}, \quad \text{(F8)}$$

and the Matsubara Green's functions for the holon and doublon at the impurity take the form

$$G_{a_d}(iv_n) = \sqrt{\frac{U}{2\sqrt{\lambda U + h^2}}} \frac{1}{iv_n - \sqrt{\lambda + \frac{h^2}{U}} + h}, \quad \text{(F9)}$$

$$G_{b_d}(iv_n) = \sqrt{\frac{U}{2\sqrt{\lambda U + h^2}}} \frac{-1}{iv_n + \sqrt{\lambda + \frac{h^2}{U}} + h}. \quad \text{(F10)}$$

With the holon and doublon operators in both the impurity and the QSL, the mean-field action S_0 now becomes

$$S_0 = -\sum_{\sigma, \omega_n} (a_\sigma^\dagger(i\omega_n) \quad f_{\sigma,\boldsymbol{R}}^\dagger(i\omega_n)) \begin{pmatrix} i\omega_n - \epsilon_0 + h & -w \\ -w & G_{f,\sigma}^{-1}(i\omega_n, \boldsymbol{R}, \boldsymbol{R}) \end{pmatrix} \begin{pmatrix} a_\sigma(i\omega_n) \\ f_{\sigma,\boldsymbol{R}}(i\omega_n) \end{pmatrix}$$

$$- \sum_{v_n} (a_d(iv_n) \quad b_d^\dagger(iv_n) \quad a_{\boldsymbol{R}}(iv_n) \quad b_{\boldsymbol{R}}^\dagger(iv_n)) \begin{pmatrix} G_{a_d}^{-1}(iv_n) & 0 & -u & -u \\ 0 & G_{b_d}^{-1}(iv_n) & -u & -u \\ -u & -u & G_a^{-1}(iv_n) & 0 \\ -u & -u & 0 & G_b^{-1}(iv_n) \end{pmatrix} \begin{pmatrix} a_d^\dagger(iv_n) \\ b_d(iv_n) \\ a_{\boldsymbol{R}}^\dagger(iv_n) \\ b_{\boldsymbol{R}}(iv_n) \end{pmatrix}. \quad \text{(F11)}$$

In the slave rotor representation, the electron at the impurity is composed of the SAF combined with the impurity holon and doublon,

$$d_\sigma^\dagger = a_\sigma^\dagger(a_d + b_d^\dagger), \quad d_\sigma = a_\sigma(a_d^\dagger + b_d). \quad \text{(F12)}$$

The electrons in the QSL are composed of the spinons combined with the QSL holons and doublons,

$$c_{\sigma,\boldsymbol{r}}^\dagger = f_{\sigma,\boldsymbol{r}}^\dagger(a_{\boldsymbol{r}} + b_{\boldsymbol{r}}^\dagger), \quad c_{\sigma,\boldsymbol{r}} = f_{\sigma,\boldsymbol{r}}(a_{\boldsymbol{r}}^\dagger + b_{\boldsymbol{r}}). \quad \text{(F13)}$$

With the holon and doublon operators, the electronic bare Matsubara Green's function that involves the impurity, the nearest-neighboring QSL site, and the coupling is constructed as

$$G_\sigma^0(i\omega_n) = \begin{pmatrix} \hat{G}_{d,\sigma}^0(i\omega_n) & \hat{T}_\sigma(i\omega_n) \\ \hat{T}_\sigma^\dagger(i\omega_n) & \hat{G}_{c,\sigma}(i\omega_n) \end{pmatrix}, \quad \text{(F14)}$$

with

$$\hat{G}_{d,\sigma}^0(i\omega_n) = -\frac{1}{\beta} \sum_{v_n} \langle a_\sigma(i\omega_n + iv_n)a_\sigma^\dagger(i\omega_n + iv_n)\rangle_0 \left\langle \begin{pmatrix} a_d^\dagger(iv_n)a_d(iv_n) & a_d^\dagger(iv_n)b_d^\dagger(iv_n) \\ b_d(iv_n)a_d(iv_n) & b_d(iv_n)b_d^\dagger(iv_n) \end{pmatrix} \right\rangle_0, \quad \text{(F15)}$$

$$\hat{T}_\sigma(i\omega_n) = -\frac{1}{\beta} \sum_{v_n} \langle a_\sigma(i\omega_n + iv_n)f_{\sigma,\boldsymbol{R}}^\dagger(i\omega_n + iv_n)\rangle_0 \left\langle \begin{pmatrix} a_d^\dagger(iv_n)a_{\boldsymbol{R}}(iv_n) & a_d^\dagger(iv_n)b_{\boldsymbol{R}}^\dagger(iv_n) \\ b_d(iv_n)a_{\boldsymbol{R}}(iv_n) & b_d(iv_n)b_{\boldsymbol{R}}^\dagger(iv_n) \end{pmatrix} \right\rangle_0, \quad \text{(F16)}$$

$$\hat{T}_\sigma^\dagger(i\omega_n) = -\frac{1}{\beta} \sum_{v_n} \langle f_{\sigma,\boldsymbol{R}}(i\omega_n + iv_n)a_\sigma^\dagger(i\omega_n + iv_n)\rangle_0 \left\langle \begin{pmatrix} a_{\boldsymbol{R}}^\dagger(iv_n)a_d(iv_n) & a_{\boldsymbol{R}}^\dagger(iv_n)b_d^\dagger(iv_n) \\ b_{\boldsymbol{R}}(iv_n)a_d(iv_n) & b_{\boldsymbol{R}}(iv_n)b_d^\dagger(iv_n) \end{pmatrix} \right\rangle_0, \quad \text{(F17)}$$

$$\hat{G}_{c,\sigma}(i\omega_n) = -\frac{1}{\beta} \sum_{v_n} \langle f_{\sigma,\boldsymbol{R}}(i\omega_n + iv_n)f_{\sigma,\boldsymbol{R}}^\dagger(i\omega_n + iv_n)\rangle_0 \left\langle \begin{pmatrix} a_{\boldsymbol{R}}^\dagger(iv_n)a_{\boldsymbol{R}}(iv_n) & a_{\boldsymbol{R}}^\dagger(iv_n)b_{\boldsymbol{R}}^\dagger(iv_n) \\ b_{\boldsymbol{R}}(iv_n)a_{\boldsymbol{R}}(iv_n) & b_{\boldsymbol{R}}(iv_n)b_{\boldsymbol{R}}^\dagger(iv_n) \end{pmatrix} \right\rangle_0. \quad \text{(F18)}$$

Those 2×2 correlators can all be obtained from the action S_0 in Eq. (F11). In this way, the impurity bare electronic Matsubara Green's function $G_{d,\sigma}^0(i\omega_n)$ is recovered as $G_{d,\sigma}^0(i\omega_n) = \sum_{i,j=1,2}[\hat{G}_{d,\sigma}^0(i\omega_n)]_{ij}$.

The spinon-chargon binding interaction in the QSL introduces new terms to the action,

$$S' = \int_0^\beta \int U_{\boldsymbol{r}} \sum_\sigma (f_{\sigma,\boldsymbol{r}}^\dagger f_{\sigma,\boldsymbol{r}} a_{\boldsymbol{r}}^\dagger a_{\boldsymbol{r}} - f_{\sigma,\boldsymbol{r}}^\dagger f_{\sigma,\boldsymbol{r}} b_{\boldsymbol{r}}^\dagger b_{\boldsymbol{r}})d\boldsymbol{r} \, d\tau, \quad \text{(F19)}$$

and now the total action is $S = S_0 + S'$. Taking the effect of the spinon-charge binding interaction into account, we can use the random phase approximation to calculate the Matsubara electronic Green's function. The resulting Matsubara electronic Green's function is

$$G_\sigma(i\omega_n) = [1 - G_{0,\sigma}(i\omega_n)\hat{U}]^{-1} G_{0,\sigma}(i\omega_n), \quad (F20)$$

with

$$\hat{U} = \begin{pmatrix} 0 & 0 & 0 & 0 \\ 0 & 0 & 0 & 0 \\ 0 & 0 & U_\mathbf{R} & 0 \\ 0 & 0 & 0 & -U_\mathbf{R} \end{pmatrix}. \quad (F21)$$

As a result, the spinon-charge binding interaction modified impurity electronic Green's function can eventually be obtained as

$$G_{d,\sigma}(i\omega_n) = \sum_{i,j=1,2} [G_\sigma(i\omega_n)]_{ij}$$

$$= G_{d,\sigma}^0(i\omega_n) + \sum_{i,j=1,2} \{\hat{T}_\sigma(i\omega_n)U_\mathbf{R}\sigma_z$$

$$\times [1 - \hat{G}_{c,\sigma}(i\omega_n)U_\mathbf{R}\sigma_z]^{-1}\hat{T}_\sigma(i\omega_n)\}_{ij}, \quad (F22)$$

and the QSL electronic Green's function is

$$G_{c,\sigma}(i\omega_n) = \sum_{i,j=1,2} \{\hat{G}_{c,\sigma}(i\omega_n)[1 - \hat{G}_{c,\sigma}(i\omega_n)U_\mathbf{R}\sigma_z]^{-1}\}_{ij}. \quad (F23)$$
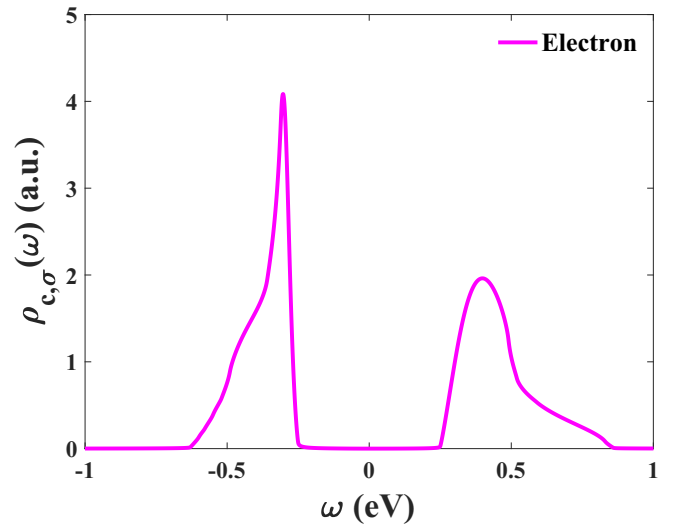

FIG. 5. The electronic spectral function $\rho_{c,\sigma}(\omega)$ in the QSL. The gauge field fluctuation-induced spinon-charge binding interaction is taken to be $U_\mathbf{R} = 0.23$ eV.

Given the same on-site spinon-charge binding interaction $U_\mathbf{R} = 0.23$ eV, the QSL electronic spectral function $\rho_{c,\sigma}(\omega) = -\frac{1}{\pi}\mathrm{Im}G_{c,\sigma}(i\omega_n \to \omega + i0^+)$ is plotted in Fig. 5. It can be seen in Fig. 5 that the on-site spinon-charge binding interaction changes the QSL electronic spectral function $\rho_{c,\sigma}(\omega)$ compared with that in Fig. 4(c), but there are no resonance peaks emerging at the Hubbard band edges.

[1] P. W. Anderson, Localized magnetic states in metals, Phys. Rev. **124**, 41 (1961).

[2] A. C. Hewson, *The Kondo Problem to Heavy Fermions* (Cambridge University Press, Cambridge, England, 1996).

[3] J. Kondo, Resistance minimum in dilute magnetic alloys, Prog. Theor. Phys. **32**, 37 (1964).

[4] I. Affleck, in *The Kondo Screening Cloud: What It Is and How to Observe It*, edited by A. Aharony and O. Entin-Wohlman (World Scientific, Singapore, 2010).

[5] G. Gruner and A. Zawadowski, Magnetic impurities in nonmagnetic metals, Rep. Prog. Phys. **37**, 1497 (1974).

[6] J. E. Gubernatis, J. E. Hirsch, and D. J. Scalapino, Spin and charge correlations around an Anderson magnetic impurity, Phys. Rev. B **35**, 8478 (1987).

[7] V. Barzykin and I. Affleck, The Kondo Screening Cloud: What Can We Learn from Perturbation Theory? Phys. Rev. Lett. **76**, 4959 (1996).

[8] I. V. Borzenets, J. Shim, J. Chen, A. Ludwig, A. Wieck, S. Tarucha, H.-S. Sim, and M. Yamamoto, Observation of the Kondo screening cloud, Nature (London) **579**, 210 (2020).

[9] J. Li, W.-D. Schneider, R. Berndt, and B. Delley, Kondo Scattering Observed at a Single Magnetic Impurity, Phys. Rev. Lett. **80**, 2893 (1998).

[10] V. Madhavan, W. Chen, T. Jamneala, M. F. Crommie, and N. S. Wingreen, Tunneling into a single magnetic atom: Spectroscopic evidence of the Kondo resonance, Science **280**, 567 (1998).

[11] S. Florens, L. Fritz, and M. Vojta, Kondo Effect in Bosonic Spin Liquids, Phys. Rev. Lett. **96**, 036601 (2006).

[12] A. Kolezhuk, S. Sachdev, R. R. Biswas, and P. Chen, Theory of quantum impurities in spin liquids, Phys. Rev. B **74**, 165114 (2006).

[13] K.-S. Kim and M. D. Kim, Kondo physics in the algebraic spin liquid, J. Phys.: Condens. Matter **20**, 125206 (2008).

[14] P. Ribeiro and P. A. Lee, Magnetic impurity in a $U(1)$ spin liquid with a spinon Fermi surface, Phys. Rev. B **83**, 235119 (2011).

[15] M. Gomilšek, R. Žitko, M. Klanjšek, M. Pregelj, C. Baines, Y. Li, Q. Zhang, and A. Zorko, Kondo screening in a charge-insulating spinon metal, Nat. Phys. **15**, 754 (2019).

[16] G. Chen and J. L. Lado, Impurity-induced resonant spinon zero modes in Dirac quantum spin liquids, Phys. Rev. Research **2**, 033466 (2020).

[17] R. Wang, Y. Wang, Y. X. Zhao, and B. Wang, Emergent Kondo Behavior from Gauge Fluctuations in Spin Liquids, Phys. Rev. Lett. **127**, 237202 (2021).

[18] S. Shen *et al.*, Inducing and tuning Kondo screening in a narrow-electronic-band system, Nat. Commun. **13**, 2156 (2022).

[19] P. A. Lee, N. Nagaosa, and X.-G. Wen, Doping a Mott insulator: Physics of high-temperature superconductivity, Rev. Mod. Phys. **78**, 17 (2006).

[20] L. Savary and L. Balents, Quantum spin liquids: A review, Rep. Prog. Phys. **80**, 016502 (2017).

[21] Y. Zhou, K. Kanoda, and T.-K. Ng, Quantum spin liquid states, Rev. Mod. Phys. **89**, 025003 (2017).

[22] K. T. Law and P. A. Lee, 1T-TaS$_2$ as a quantum spin liquid, Proc. Natl. Acad. Sci. (USA) **114**, 6996 (2017).

[23] W.-Y. He, X. Y. Xu, G. Chen, K. T. Law, and P. A. Lee, Spinon Fermi Surface in a Cluster Mott Insulator Model on a Triangular Lattice and Possible Application to 1T-TaS$_2$, Phys. Rev. Lett. **121**, 046401 (2018).

[24] C.-K. Li, X.-P. Yao, J. Liu, and G. Chen, Fractionalization on the surface: Is type-II terminated 1T-TaS$_2$ surface an anomalously realized spin liquid? arXiv:2109.08093.

[25] M. Klanjšek, A. Zorko, R. Žitko, J. Mravlje, Z. Jagličič, P. K. Biswas, P. Prelovšek, D. Mihailovic, and D. Arčon, A high-temperature quantum spin liquid with polaron spins, Nat. Phys. **13**, 1130 (2017).

[26] S. Qiao *et al.*, Mottness Collapse in 1T-TaS$_{2-x}$Se$_x$ Transition-Metal Dichalcogenide: An Interplay Between Localized and Itinerant Orbitals, Phys. Rev. X **7**, 041054 (2017).

[27] C. J. Butler, M. Yoshida, T. Hanaguri, and Y. Iwasa, Mottness versus unit-cell doubling as the driver of the insulating state in 1T-TaS$_2$, Nat. Commun. **11**, 2477 (2020).

[28] C. J. Butler, M. Yoshida, T. Hanaguri, and Y. Iwasa, Doublonlike Excitations and Their Phononic Coupling in a Mott Charge-Density-Wave System, Phys. Rev. X **11**, 011059 (2021).

[29] J. Lee, K.-H. Jin, and H. W. Yeom, Distinguishing a Mott Insulator from a Trivial Insulator with Atomic Adsorbates, Phys. Rev. Lett. **126**, 196405 (2021).

[30] Y. Chen *et al.*, Strong correlations and orbital texture in single-layer 1T-TaSe$_2$, Nat. Phys. **16**, 218 (2020).

[31] W. Ruan *et al.*, Evidence for quantum spin liquid behaviour in single-layer 1T-TaSe$_2$ from scanning tunnelling microscopy, Nat. Phys. **17**, 1154 (2021).

[32] Y.-Chen *et al.*, Evidence for a spinon Kondo effect in cobalt atoms on single-layer 1T-TaSe$_2$, arXiv:2202.07224.

[33] V. Madhavan, W. Chen, T. Jamneala, and M. F. Crommie, Local spectroscopy of a Kondo impurity: Co on Au(111), Phys. Rev. B **64**, 165412 (2001).

[34] S.-S. Lee and P. A. Lee, $U(1)$ Gauge Theory of the Hubbard Model: Spin Liquid States and Possible Application to κ-(BEDT-TTF)$_2$Cu$_2$(CN)$_3$, Phys. Rev. Lett. **95**, 036403 (2005).

[35] S. Florens and A. Georges, Quantum impurity solvers using a slave rotor representation, Phys. Rev. B **66**, 165111 (2002).

[36] S. Florens and A. Georges, Slave-rotor mean-field theories of strongly correlated systems and the Mott transition in finite dimensions, Phys. Rev. B **70**, 035114 (2004).

[37] A. M. Polyakov, Quark confinement and topology of gauge theories, Nucl. Phys. B **120**, 429 (1977).

[38] M. Hermele, T. Senthil, M. P. A. Fisher, P. A. Lee, N. Nagaosa, and X.-G. Wen, Stability of $U(1)$ spin liquids in two dimensions, Phys. Rev. B **70**, 214437 (2004).

[39] S.-S. Lee, Low-energy effective theory of Fermi surface coupled with $U(1)$ gauge field in $2+1$ dimensions, Phys. Rev. B **80**, 165102 (2009).

[40] X.-G. Wen and P. A. Lee, Theory of Underdoped Cuprates, Phys. Rev. Lett. **76**, 503 (1996).

[41] P. A. Lee, N. Nagaosa, T.-K. Ng, and X.-G. Wen, SU(2) formulation of the t-J model: Application to underdoped cuprates, Phys. Rev. B **57**, 6003 (1998).

[42] E. Tang, M. P. A. Fisher, and P. A. Lee, Low-energy behavior of spin-liquid electron spectral functions, Phys. Rev. B **87**, 045119 (2013).

[43] Y. Cao *et al.*, Correlated insulator behaviour at half-filling in magic-angle graphene superlattices, Nature (London) **556**, 80 (2018).

[44] Y. Cao *et al.*, Unconventional superconductivity in magic-angle graphene superlattices, Nature (London) **556**, 43 (2018).

[45] L. Balents, C. R. Dean, D. K. Efetov, and A. F. Young, Superconductivity and strong correlations in moiré flat bands, Nat. Phys. **16**, 725 (2020).

[46] D. Podolsky, A. Paramekanti, Y. B. Kim, and T. Senthil, Mott Transition between a Spin-Liquid Insulator and a Metal in Three Dimensions, Phys. Rev. Lett. **102**, 186401 (2009).

[47] C. P. Nave, S.-S. Lee, and P. A. Lee, Susceptibility of a spinon Fermi surface coupled to a U(1) gauge field, Phys. Rev. B **76**, 165104 (2007).